Hydrocolloids

Zhang, Yan; Baiocco, Dan; Mustapha, Abdullah; Zhang, Xiaotong; Yu, Qinghua; Wellio, Gilmore; Zhang, Zhibing; Li, Yongliang

DOI:
10.1016/j.cej.2019.123028

Document Version
Peer reviewed version

Citation for published version (Harvard):
Zhang, Y, Baiocco, D, Mustapha, A, Zhang, X, Yu, Q, Wellio, G, Zhang, Z & Li, Y 2020, 'Hydrocolloids: nova materials assisting encapsulation of volatile phase change materials for cryogenic energy transport and storage', *Chemical Engineering Journal*, vol. 382, 123028. https://doi.org/10.1016/j.cej.2019.123028

Hydrocolloids: Nova Materials Assisting Encapsulation of Volatile Phase Change Materials for Cryogenic Energy Transport and Storage

Yan Zhang [a,b], *Daniele Baiocco* [b], *Abdullah Naseer Mustapha* [a,b], *Xiaotong Zhang* [b], *Qinghua Yu* [a], *Gilmore Wellio* [a,b], *Zhibing Zhang** [b], *Yongliang Li** [a]

[a] Birmingham Center for Energy Storage, School of Chemical Engineering, University of Birmingham, Edgbaston, Birmingham, West Midlands, B15 2TT, United Kingdom

[b] Micromanipulation and Microencapsulation Research Group, School of Chemical Engineering, University of Birmingham, Edgbaston, Birmingham, West Midlands, B15 2TT, United Kingdom

* E-mail: Z.Zhang@bham.ac.uk E-mail: Y.Li.1@bham.ac.uk

KEYWORDS: capsules, cryogenic, hydrocolloids, PCM, thermal energy storage, volatile

Abstract

A series of norm-defying hydrocolloid emulsifiers is reported for the challenging task of outstanding long-term retention of volatile cryogenic phase change materials (cryoPCM) in high-payload capsules. Their identification lifted previously imposed restrictions on emulsifier selection in order to fine-tune the mechanical and barrier properties, shell thickness, size and

surface roughness of capsules. The exceptionally large payload in terms of both volume (~ 97 *vol*.%) and weight (~ 95 *wt*.%), superb long-term retention capability tested at ambient conditions up to 30 days, as well as the surprising cryo-temperature survival of synthesized capsules promote them as immensely efficient candidate carriers for cryogenic thermal energy storage and transport. Utilization of appropriate hydrocolloids and concentrations not only bestows the thermosetting polymeric shells with flexibility, but also eliminates the majority of imbedding satellite particles producing exterior surfaces comparable to a two-step synthesis route ever reported. Promising fatigue resistance within an extreme dynamic temperature range between 20 ºC to -140 ºC during preliminary cycling tests has been demonstrated via direct observation of capsule buckling and restoration. Such findings provide fundamental insights into achieving superior capsule quality and their far-reaching impacts beyond cryogenic energy storage on applications such as less harsh cold chain logistics, electrophoresis displays, battery safety management and self-healing materials.

1. Introduction

Cryogenic thermal energy storage and transport has increasingly appealed to researchers in recent years to improve the performance of cryogenic systems and processing. Two unique grid-scale energy storage technologies, liquefied air and pumped thermal electricity storage, both require an aid to improve their overall performances.[1-3] The development of a large-scale, efficacious and cost-effective cold storage approach will not only have positive impacts on liquefaction of air or natural gas and cold recovery for re-gasification in the cryogenic industry,[4-5] but also enable demand management and optimization of electricity consumption patterns for more efficient utilization of intermittent renewable energy sources to reduce carbon footprint.[6-8]

Packed beds of quartzite are commonly used for cryogenic energy storage incorporating intermediate heat transfer cycles for energy transport.[9-10] However, the small thermal storage density, low efficiency and poor flexibility of packed beds appeal for better solutions.[11-12] Microencapsulated phase change material (MPCM) slurries, formed by uniformly dispersing MPCM capsules into a carrier fluid, can overcome the aforementioned drawbacks through multiple advantages. MPCM slurries not only offer high thermal storage density combining both the latent heat of PCM and sensible heat of the carrier liquid,[13] but also facilitate high-efficiency heat transfer process via the miscellaneous particle-liquid, particle-particle and particle-wall interactions while being transported by pumping due to their good fluidity. More importantly, the temperature profile of the MPCM slurry undergoing an isobaric phase change process can be designed by adding different micro-sized capsules to match the abrupt specific heat change of transcritical/supercritical fluids in order to minimize the exergy loss.

Capsules have long enjoyed their popularity in drug carrier design,[14-16] fragrance retention,[17-19] and self-healing materials,[20-22] while seeking niche application frontiers in reaction scavengers,[23] lithium-ion batteries,[24-27] fuel cells,[28] carbon capture,[29] and thermal energy storage.[30-31] In most cases, the active ingredients are non-volatile liquids or even solids at room temperature,[32] which extenuates the leakage problem and endorses a diverse range of synthesis routes. Cryogenic phase change materials (cryoPCM) are a species bearing boiling points typically below 100 ºC, placing them at the dividing boundary of 50-100 ºC between volatile organic compounds (VOC) and very volatile organic compounds (VVOC).[33-35] We hereby categorize cryoPCM as VOC following a defining vapor pressure of 0.13~101.3 kPa at 20 ºC.[33] Research in VOC cryoPCM encapsulation is eminently scanty in the literature due to challenges in their long-term containment and stability within the extreme temperature range. Advancement in the retention of

VOC is urgently required due to soaring demands for cold storage unfulfilled by research stagnancy.

In order to fulfill the requirements for cryogenic energy transport and storage, one must address three challenges on the capsule level: (1) exceptional impermeability ideally with nil leakage; (2) supreme mechanical durability to withstand the extreme temperature range; and (3) excellent thermal performance such as large enthalpy of fusion, thermal conductivity *etc*. Despite their equivalent significance, one must address the three deliverables in the aforementioned priority sequence. Repeated energy storage and release are only guaranteed on achieving impeccable barrier properties, along with sublime mechanical strength and fatigue resistance within a prodigious temperature range. Only upon accomplishing these two first would improving thermal properties of intact capsules become meaningful. Even though our ultimate target is for cryogenic energy storage and transport, the scientific findings on various properties of the capsules over the wide compatible temperature range are of universal interest to less harsh cold-chain logistic applications.

To inherit from metallization of capsule shells for long-term retention of volatile cargos,[36-37] the first-level encapsulation must provide a decently non-permeable template to at least temporarily alleviate substantial leakage before any meaningful subsequent coating completes. Interfacial polymerization could produce polyurea and polyurethane elastomers with sub-zero glass transition temperatures T_g,[38-40] imparting elasticity in shells favorable for low temperatures. However, the mechanism of increasing free volume within polymer network for molecular reconfiguration without covalent bonding rupture[41] compromises shell impermeability. Producing large capsules with shell thicknesses to tens of microns could mitigate the concern,[42] but at the expense of capsule payload. Common silicone-based materials such as poly(dimethyl

siloxane) (PDMS) used for microfluidic devices usually swell in nonpolar solvents,[43-44] rendering them incompatible as shell materials with prevalently hydrocarbon-based cryoPCM. Solvent extraction imposes stringent restrictions on ingredient mixing ratios, interfacial tension relationships and the boiling point of oil phases in order to produce core-shell structured capsules.[45-47] This would limit the flexibility in controlling capsule payload, size and shell thickness even if possible. Sol-gel processes produce strong capsules with low volatility PCM.[29, 48-50] Subsequent annealing at elevated temperatures to reduce porosity [51] would accelerate cryoPCM evaporation. We speculate that in situ polymerization most likely qualify as a promising candidate among available encapsulation routes owing to the highly cross-linked thermoset polymer network.

In situ polymerization utilizes an oil-in-water (O/W) emulsion as a template, while pH in combination with heat initiates the polymerization from the aqueous continuous phase to form shells encapsulating these droplets. Depending on the cross-linking precursors, two synthesis routes have been developed: (1) a two-step route making use of a precondensate under alkaline conditions first followed by subsequent polymerization from such a precondensate in acidic environment,[52-55] and (2) a one-step route eliminating the synthesis of such a precondensate and polymerizing directly from monomers from the aqueous phase.[56-59] Researchers have predominantly used the two-step route in PCM encapsulation with amino resins for thermal energy storage in favor of the simpler one-step regardless,[53-55, 60-64] likely owing to its less ease of control due to sensitivity to emulsifiers of the latter.[58-59]

In this paper, we report a series of nova emulsifiers, also known as hydrocolloids, and demonstrate the long-term retention of volatile cryoPCM with their assistance. These newly identified materials facilitate us in achieving the first two deliverables in conquering the summit

of cryogenic energy storage and transport – low permeability and good mechanical properties. More importantly, we investigate and propose the requirement for emulsifier selection to make such a one-step route a success for other applications.

2. Materials and methods

2.1. Materials

Poly(acrylic acid) (Sigma-Aldrich 306215, average M_v ~ 1,250,000), poly(vinyl alcohol) (Sigma-Aldrich 363170, M_w 13,000 ~ 23, 000, 87 ~ 89% hydrolyzed), poly(ethylene-alt-maleic anhydride) (Sigma-Aldrich 188050, average M_w 100,000 ~ 500,000), gelatin from porcine skin (Sigma-Aldrich 48722), chitosan (Sigma-Aldrich 448877, medium molecular weight), methylcellulose (Sigma-Aldrich M0262, viscosity 400 cP), locust bean gum from Ceratonia silique seeds (Sigma-Aldrich G0753), pectin from apple (Sigma-Aldrich 76282), xanthan gum from Xanthomonas campestris (Sigma-Aldrich G1253), agar for microbiology (Sigma-Aldrich 05039), polyacrylamide (Sigma-Aldrich 749222, average M_n 150,000), polyethylenimine (branched, average M_w ~ 25,000 by LS, average M_n ~ 10,000 by GPC), urea (Sigma-Aldrich UK, U5128, ACS reagent grade 99.0-100.5%), resorcinol (Sigma-Aldrich UK, 398047, ACS reagent, ≥99.0%), ammonium chloride (Sigma-Aldrich UK, A9434, for molecular biology, ≥99.5%), Nile red (Sigma-Aldrich 72485, for microscopy), formaldehyde (Sigma-Aldrich 47608, for molecular biology, BioReagent, ≥36.0% in H_2O), heptane (Sigma-Aldrich 246654, anhydrous 99%), 1-octene (Alfa Aesar A11146, 97%), Dowtherm J (DOW Chemical), catechol (Alfa Aesar A10164.30, 99%), and hydroquinone (Alfa Aesar A11411.30, 99%).

2.2. Capsule synthesis

All capsules were synthesized via the one-step in situ polymerization published elsewhere.[55-56] For standard synthesis, the aqueous phase was prepared by dissolving the emulsifier first at an appropriate concentration into 150 g deionized water and then 2.50 g urea, 0.25 g resorcinol and 0.25 g NH_4Cl. The specific dissolution method depends on the selected emulsifier. For gelatin, it was dissolved by heating to 50 ºC and then maintained at the temperature under stirring for 5 min, and cooled down naturally. Chitosan was dissolved by adjusting pH to 3.5 and magnetic stirring for 12 h. Methylcellulose, pectin and xanthan gum were all dissolved using high shear homogenization at 3000 rpm for 5 min and ultrasonication for 5 min for degassing air bubbles. Locust bean gum was boiled inside a round bottom flask heated via an electrical mantle for 2 h with a reflux configuration and cooled down naturally. Agar was boiled inside a round bottom flask heated up to 80 ºC for 30 min with a reflux configuration and cooled down naturally. Polyacrylamide and polyethylenimine were dissolved within an ultrasonic bath for 1 h and 0.5 h, respectively. The initial pH of all prepared solutions was adjusted to 3.5 with HCl solutions. When the fluorescent sensing method was required, Nile red was dissolved in heptane via ultrasonication for 10 min prior to emulsification. The oil phase was emulsified in the aqueous phase inside a 200 mL glass beaker on a high shear homogenizer (1200 rpm for 20 min). The produced emulsion was then transferred into a 250 mL jacketed beaker connected with a water bath, and maintained under agitation at 600 rpm on a mechanical stirrer at 20 °C. 6.5 mL formaldehyde was injected into the emulsion and the beaker opening was covered with aluminum foil for prevent evaporation. The polymerization was initiated by heating up the circulating water to 55 °C and maintained at the temperature for 4 h. The final products were centrifuged 4 times and vacuum filtered with 5 L of distilled water. For the special case of

catechol and hydroquinone, 2.50 g of each alternative was used to replace resorcinol while all rest parameters remained identical.

2.3. Bright-field optical (OM) and fluorescence microscopy (FM)

Bright-field optical microscopy images were captured on a Leica DMRBE microscope with PL FLUOTAR 5×/0.12 and 10×/0.30 lens. The fluorescent color of capsules under excitation was investigated on the Leica microscope with a CoolLED pE-300 series illumination system. A H3 filter cube (BP420-490) with a dichromatic mirror (510) and suppression filter (LP 515) was selected as the configuration. The blue excitation light maximum peaked at around $\lambda_{ex\ max}$ = 460 nm.

2.4. Bright-field optical (OM) microscopy for buckling observation

The observation of capsule buckling was performed on a Zeiss AXIO A1 microscope (Zeiss 20 ×/0,22 DIC ∞/0 objective lens) inside a Linkam stage T95-PE with liquid nitrogen cooling.

2.5. Scanning electron microscopy (SEM)

SEM micrographs were captured with a Hitachi TM3030 electron microscope with a backscattered electron (BSE) detector in EDX mode. High resolution SEM for shell thickness characterization was carried out on a Philips XL30 environmental SEM (ESEM-FEG) using a secondary electron (SE) detector at an acceleration voltage of 10 kV. Samples were coated with Au prior to observation.

2.6. Electrophoresis mobility

The electrophoresis mobility results were acquired from Malvern Zetasizer Nano ZS. The disposable folded capillary zeta cell (DTS1070) were used and connected with an automatic

titrator (Malvern MPT-2) for pH adjustment (2~12) via 1 M NaOH and HCl solutions. Three replicates were produced for each hydrocolloids.

2.7. Attenuated total reflection Fourier-transform infrared spectroscopy (ATR-FTIR)

ATR-FTIR spectra were acquired on a Bruker Tensor 27 spectrometer. Powder samples were firstly pressed into tablets with a punch die on a Lloyd X mechanical tester (LS100 Plus) with a loading capacity of 100 kN. The samples were loaded at 80 kN at 10 mm/min for 120 s and then the force was relieved. Spectra resolution was 4 cm^{-1}, both background and sample scan times were 256 times, acquiring data from 400 to 4000 cm^{-1}.

2.8. Bulk rheology

A HR-1 Discover Hybrid Rheometer (TA Instrument, UK) was used to measure the shear viscosity (dynamic viscosity) of the bulk aqueous phase. 8.5 ml of the aqueous solution was loaded via a transfer pipette into a TA Peltier concentric cylinder geometry, with a double gap rotor and cup configuration. The measurements were carried out at a preset temperature of 25 ºC within the shear rate range of 100 ~ 1000 s^{-1}.

2.9. Interfacial rheology

A Sinterface Profile Analysis Tensiometer PAT1M was used to measure the interfacial dilatational viscosity at heptane-water interfaces at the presence of miscellaneous emulsifiers. The aqueous phase was inserted into an OG Hellma Optical Glass Cuvette (50 ± 0.5 mm light path) (Hellma Analytics, Germany), while heptane was maintained at a constant volume of 25 µl, using an inverted capillary (ϕ 3 mm). Measurement was initiated when interfacial tension became constant. The period for the sinusoidal harmonic oscillation procedure was set to be 100 s, with a 10 % amplitude. Each sample was measured 5 times.

2.10. Interfacial tension

A pendant drop method was used on a KRÜSS drop shape analyzer (DSA30) to study the interfacial tension between heptane and various hydrocolloid emulsifier solutions. The aqueous hydrocolloid solutions were the bulk phase inside a glass cuvette. Heptane was dispensed through a 1 mL syringe via a J-shaped stainless steel needle inside the aqueous phase to form an upward pendant drop. The shape was analyzed via KRÜSS Advance software. Data collection frequency was every minute and all tests were performed for 6 hours. Data acquired during the last 3 hours were used for calculating the means of interfacial tension.

2.11. Payload characterization

Payload was characterized by rupturing the capsules to release the volatile heptane and weigh the mass difference before and afterwards. 0.5 g of dry capsules were decanted into a punch die used for making tablets during ATR-FTIR sample preparation. A tablet was compressed following the same loading curve as specified above. The punch die was then transferred into a fume hood for handling. The tablet was dried for 30 min before weighing. For the payload characterization, 3 replicates were performed.

2.12. Micromanipulation

Micromanipulation was performed on a self-built system with a CCD camera. A force transducer 403A (Aurora Scientific Inc. serial No. 1569) with a sensitivity of 0.453 mN/V was mounted with a polished glass needle in the diameter of approximately 125 μm glued on. The translation velocity was 2 μm/s. Samples were dispensed via pipettes onto a pre-cut glass substrate which were fitted onto the system and dried to achieve dispersion. Compliance of the system was tested 5 times prior to measurement and the average was calculated to compensate displacement for

more accurate results. For each sample, 60 randomly selected capsules were compressed until either they broke or the maximum load was reached.

2.13. Thermal cycling

Thermal cycling for the fluorescence microscopy observation was carried out on a TA Instruments DIL 806 dilatometer coupled with a PolyScience water bath and a liquid nitrogen dewar for cooling. Samples were prepared on microscope glass slides: an ultrathin double-sided tape (Tesa® 68557 10 μm d/s ultrathin PET tape by courtesy of Tesa®) layer was bonded onto the glass slide and dry capsules were sprinkled on top. Loosely attached particles were blown off with an air gun gently. Before thermal cycling, they were observed under OM/FM and the glass slides were placed inside the dilatometer chamber after images were captured. The thermal cycling was performed 10 times with 25 L liquid nitrogen from room temperature to -140 ºC at a heating/cooling rate of 7.5 ºC/min. The samples were then observed under OM/FM at the same locations as previously for comparison. For SEM observation, instead of using glass slides, the aluminum stubs with carbon adhesive pads were used.

2.14. Differential Scanning Calorimetry (DSC)

The phase transition of heptane-PUF capsules was monitored on Mettler Toledo DSC 3 STARe with liquid N_2 as the coolant. Heating/cooling rates were 5 ºC/min, and N_2 gas flow was 20 mL/min. The temperature profile was cooling down from -60 ºC to -140 ºC at -5 ºC/min and holding an isothermal section for 5 min prior to heating up at 5 ºC/min to -60 ºC again. Capsules were sealed inside 40 μL aluminum crucibles without pin holes.

2.15. Liquid chromatography- electrospray ionization mass spectrometry (LC-MS)

The molecular weights of water-soluble oligomer residue of the supernatants were injected into a Thermo Finnigan Surveyor HPLC column with 0.05 % acetic acid and water as solvent A, and 0.05 % acetic acid and acetonitrile as solvent B, and analyzed on a Thermo Scientific LCQ fleet Ion Trap LC/MS. The scouting gradient was set at 100 % A to 100 % B over a total time of 20 minutes. The samples were then transferred through the ion transfer capillary into the MS, set at 10 V and a temperature of 250 °C. The electrospray ionization needle (ESI) was set with a voltage of 5 kV, with a 60º angle to the capillary. A mass-charge ratio m/z within 50~2000 was acquired.

3. Results and discussion

Amino resin microcapsules with a model cryoPCM heptane presented in this work were produced via a one-step in situ polymerization route because of its simplicity of operation without pre-condensate synthesis. We observed the unique role emulsifiers played in cryoPCM retention despite their low concentrations added when adopting such a synthesis route.

3.1. Common polymeric emulsifiers – High-leakage capsules

Even though in situ polymerization is speculated to be the most promising candidate, the challenge remains for long-term containment of the VOC cryoPCM. Poly(ethylene-*alt*-maleic anhydride) (PEMA) has been extensively used as the emulsifier in the encapsulation of nonvolatile core cargos,[52-54] but our newly developed fluorescent sensing[55] (Figure 1 (a), see Supporting Information fluorescent sensing method for details) revealed its very limited retention ability for heptane (Figure 1 (b)). This screening method is based on the different color indications upon retention (1) and leakage (0) of the core, which are green for 1 and red for 0 in a heptane-Nile red system. The fast and effective qualitative method enabled us to focus on screening appropriate emulsifiers quickly without undertaking further unnecessary

characterization when the retention was unsuccessful. Neither poly(vinyl alcohol) (PVOH, Figure 1 (c)) nor poly(acrylic acid) (PAA, Figure 1 (d)) meaningfully improved the retention. Capsules produced with such emulsifiers possessed either porous shell structures with visible cavities or rough surfaces with numerous satellite particles (Figure 1 (b)-(d) SEM). Varying their molecular weights or concentrations did not yield noticeable difference. These common polymeric emulsifiers do not contribute to sufficiently dense structures to inhibit the evaporation of much smaller heptane molecules.

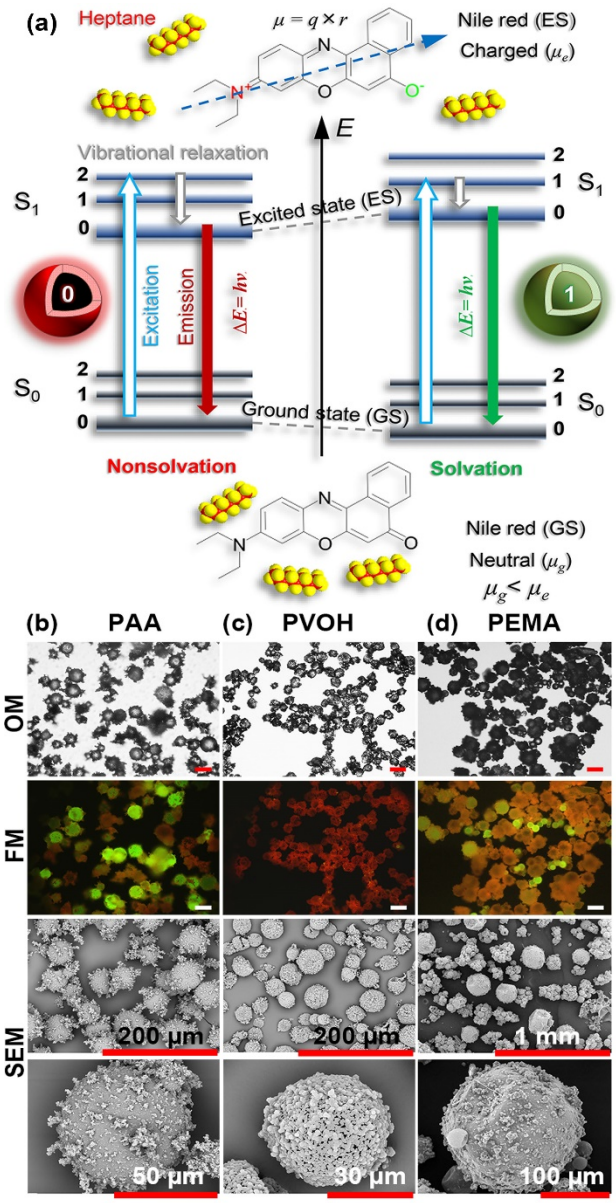

Figure 1 (a) Skematic illustration of the Jablonski diagram and molecular interactions for the developed fluorescent method to rapidly determine heptane retention (1) and leakage (0). For the case of retention (1), the large dipole moment $\mu=q\times r$ (q is charge, r is charge separation distance) of excited Nile red in heptane is rapidly destablized in nonpolar heptane generating emission photons in the green visible spectrum for the case of leakage (0), emission photon energies are reduced due to nonradiative decays and fluorescence quenching; bright-field (OM) (scale bars 50 µm), fluorescence (FM) (scale bars 50 µm) and scanning electron microscopy (SEM) images of freshly-dried Nile-red-stained microcapsules containing heptane as the core cargo produced with (b) 0.03 *wt.*% PEMA, (c) 0.1 *wt.*% PVOH and (d) 0.1 *wt.*% PAA as the emulsifier. Green and red (orange) emission colors correspond to the retention and loss of heptane respectively.

3.2. Hydrocolloid emulsifiers – High-payload capsules

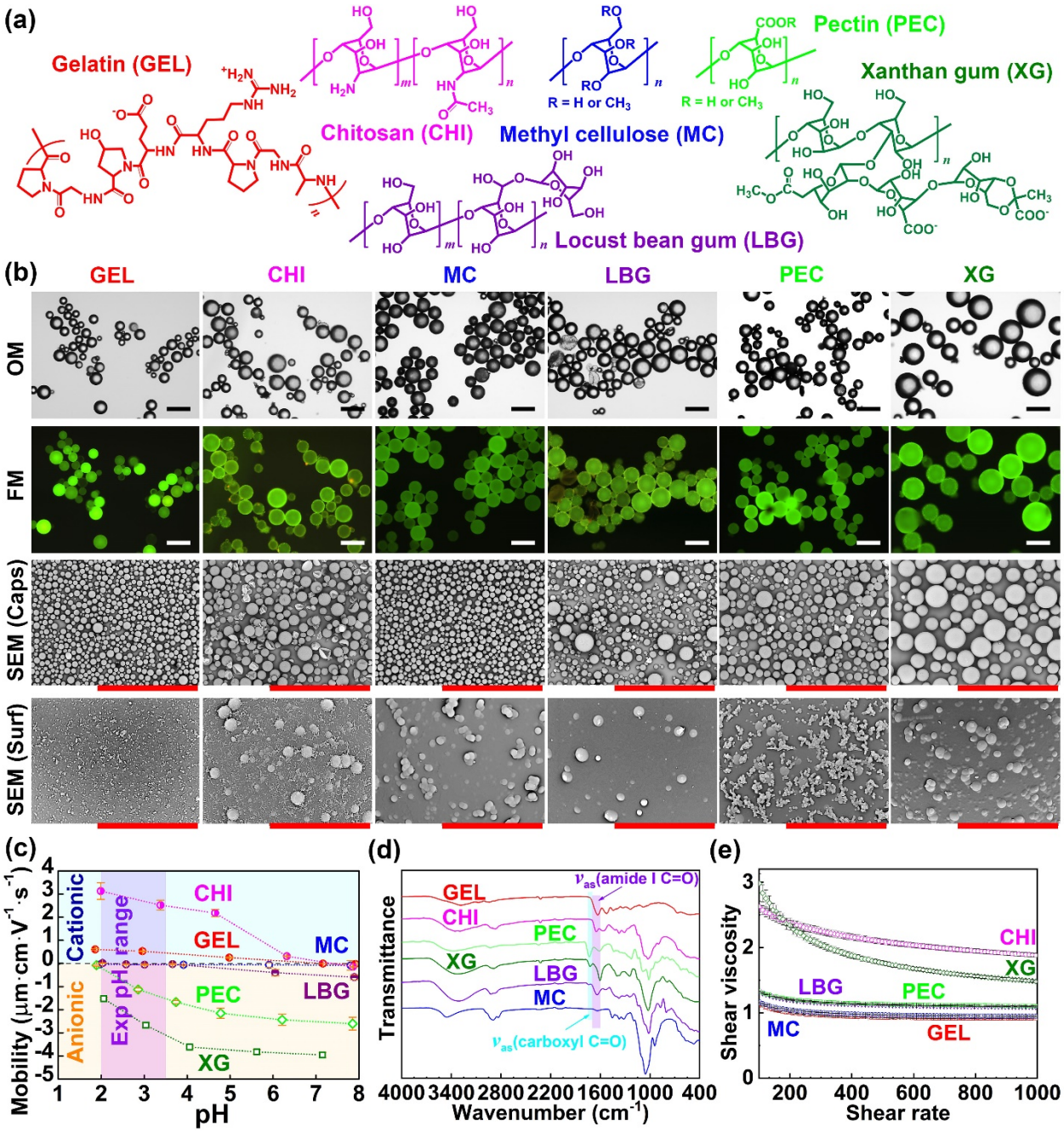

Figure 2 (a) Principal chemical structures of hydrocolloids selected for capsule synthesis: gelatin (GEL), chitosan (CHI), methylcellulose (MC), locust bean gum (LBG), pectin (PEC) and xanthan gum (XG); (b) OM (scale bars 100 μm), FM (scale bars 100 μm) and SEM (capsule morphology (caps) scale bars 1 mm, capsule exterior surfaces (surf) scale bars 20 μm) images of microcapsules synthesized by 0.02 *wt.*% of corresponding hydrocolloid emulsifiers 24 h after drying; (c) electrophoretic mobility of tested hydrocolloids in water within pH 2~12 (solution concentration 0.1 *wt.*%); (d) attenuated total reflectance Fourier-transform infrared spectroscopy (ATR-FTIR) spectra of hydrocolloids highlighting carbonyl bands at v_{as} (carboxyl C=O) = 1680~1740cm^{-1} and v_{as} (amide I C=O) = 1600~1700cm^{-1}); (e) bulk shear viscosity of 0.02 *wt.*% hydrocolloid solutions.

Our success with polysaccharides[56] prompted us into considering hydrocolloids as emulsifier substitutes. We selected gelatin (GEL), chitosan (CHI), methyl cellulose (MC), locust bean gum (LBG), pectin (PEC) and xanthan gum (XG) for demonstration. Figure 2 (a) sketches their principal chemical structures, and Table 1 tabulates their physical and chemical properties. The green fluorescent emission colors confirmed the successful retention of heptane with all six hydrocolloids (Figure 2 (b)). One attractive feature of these capsules is their free-flowing behavior after washing off excessive hydrocolloids and oligomers (SI Video 1~3), which is essential for post-processing such as surface chemistry tailoring and multi-layered coating. Figure 2 (b) also insinuates good mechanical strength and low shell permeability to withstand the SEM vacuum conditions. Selected hydrocolloids have also been tested successful with other small volatile PCM molecules such as 1-octene and xylene (Figure S1). Most importantly, the majority of capsules had high payloads over 80 *wt*.% (Table 1), undeterred by the large core-shell density discrepancy ($\rho_{C_7H_{16}}$ = 0.6795 g·cm^{-3} at 25 ºC [57], $\rho_{polymer}$ =1.15 ~ 1.19 g·cm^{-3} [58]), with an estimated core volume proportion of 78~97 *vol*.%. The high payload empowers such capsules to qualify for efficient carriers of functional cargos for self-healing and thermal energy storage materials.

Table 1 Physical and chemical properties of hydrocolloids selected for encapsulation, along with the yield, payload and encapsulation efficiency of produced microcapsules

Hydrocolloid solutions	Functional groups [a]			Surface activity	Gelling [c]	Charge [d]	Yield [e]	Payload [e]	Encapsulation efficiency [e]
	-COOH	-OH	-NH_2	(IFT [b] mN·m^{-1})			(*w*/*w*)	(*w*/*w*)	(*w*/*w*)
Gelatin (GEL)	Yes	Yes	Yes	Adsorbing (22.4)	Yes (Cold-set gelation)	+	36 ± 4 %	92 ± 1 %	63 ± 5 %
Chitosan (CHI)	No	Yes	Yes	Weak (23.7)	No (Synergy interaction)	+	30 ± 7 %	94 ± 1 %	50 ± 13 %
Methyl cellulose (MC)	No	Yes	No	Adsorbing (19.2)	Yes (Heat-set gelation)	Neutral	40 ± 6 %	83 ± 1 %	60 ± 9 %
Locust bean gum (LBG)	No	Yes	No	Weak (N/A)	No (Synergy interaction)	Neutral	31 ± 6 %	78 ± 2 %	35 ± 8 %
Xanthan gum	Yes	Yes	No	Non-adsorbing	No (Synergy	−	16 ± 4 %	91 ± 1 %	30 ± 6 %

(XG)				(43.1)	interaction)				
Pectin (PEC)	Yes	Yes	No	Weak (23.9)	No (Ionotropic gelation)	–	18 ± 4 %	86 ± 1 %	28 ± 6 %

a) from hydrocolloid molecules not contaminants; b) concentration 0.02 *wt*.%; c) without other additives; d) pH 2~3.5; e) yield was calculated by the weight of harvested dry capsules over the that of all materials used for synthesizing the core and shell excluding water; payload was calculated by dividing the weight of encapsulated core heptane by that of harvested dry capsules; encapsulation efficiency was calculated as the proportion between encapsulated heptane and its total consumption during emulsification.

We discovered the following compelling findings in the one-step in situ polymerization: (Ⅰ) there is no correlation between the hydrocolloid charge type and successful encapsulation. This immediately broke the mold of predominantly using anionic polyelectrolytes in the literature[52-54, 59-64] and diversified emulsifier options. Cationic (GEL and CHI), anionic (PEC and XG) and electrostatically neutral hydrocolloids (MC and LBG) within the experimental pH range, confirmed by electrophoretic mobility tests in Figure 2 (c), all proved to be constructive; (Ⅱ) carboxylic or anhydride moieties in hydrocolloids are not essential. Combination of electrophoretic mobility analysis (Figure 2 (c)) and FTIR spectroscopy (Figure 2 (d)) confirmed no such moieties in MC (see Figure S2 for detailed analysis). This finding challenges the practice of predominantly favoring carboxyl- or anhydride-bearing polyelectrolytes,[53] and broadens the emulsifier range even further; (Ⅲ) excellent surface activity is not necessarily required. Heptane-water interfacial tension (IFT) was measured via the pendant drop method to be 48.1 ± 0.7 $mN \cdot m^{-1}$ (25 ºC), in agreement with literature.[65-66] 0.02 *wt*.% XG exhibited merely nominal surface activity (43.1 ± 0.5 $mN\,m^{-1}$, Figure S3), nevertheless produced fairly decent capsules. It must be noted, however, that stabilization of the liquid-liquid interface where encapsulation occurs is a prerequisite. This finding, in no way, concludes emulsion stability is irrelevant since other effects (*e.g*. steric hindrance, electrostatic repulsion) can still contribute to emulsion stabilization.

These anomalous findings not only provided new insights into the shell formation mechanism, but also lifted previously imposed restrictions on emulsifier selection. A broadened range of materials enables fine-tuning capsule surface roughness, size and mechanical properties for miscellaneous applications. For instance, the surface roughness would affect the optical properties in electrophoresis displays,[54, 67] which can be adjusted via hydrocolloid type and concentrations. Synergistic effects between hydrocolloids, such as agar with LBG or XG with galactomannans (LBG and guar gum),[68-69] may enable further tuning mechanical properties.

3.3. Surface morphology and shell thickness

In order to maximize hydrocolloid diversity and reduce experiments for succeeding investigations, GEL, MC and XG were selected in accordance with their properties listed in Table 1 and miscellaneous concentrations were tested. Decreasing hydrocolloid concentration ameliorated capsule survival upon drying (Figure 3 (a)). Shells as thin as 190 nm were achieved, and lower concentrations produced thick shells close to 1 μm. Thickness can be simply tuned by varying hydrocolloids or their concentration. Capsule sizes were insensitive to hydrocolloid concentrations except for XG (Figure 3 (a)), which likely originated from the superior surface activities of MC and GEL (Table 1).

Hydrocolloid emulsifiers significantly reduced the outer rough region, characteristic of shells formed with common polymeric emulsifiers,[52, 61] into discrete imbedding particles, which could further be eliminated (0.05 ~ 0.1 *wt*.% GEL in Figure 4). Figure 3 (c) discloses clean and sharp fracture textures of thick shells (0.01 *wt*.% XG and MC), as opposed to their slightly rough-looking thin counterparts (0.1 *wt*.% XG and MC). This is the first indication of shell embrittlement with rising thickness.

XG was more effective in viscosity modification (Figure 3 (d)) due to its molecules forming an orderly network of intermolecular aggregates and entanglements via hydrogen bonding (−OH···H) in solution.[69] Higher XG concentrations did deteriorate capsule quality likely as a result of thinner shells leading to weaker mechanical strength and collapsing after drying. Hydrocolloid concentration remarkably affected capsule exterior surface morphology (Figure 4). GEL produced relatively smooth surfaces at all concentrations investigated in this work, and imbedding particles were rarely seen at concentrations above 0.05 *wt*.%. This yielded very smooth capsule surfaces comparable to the two-step method,[70] but ever achieved with the one-step route to our best knowledge. Even at a low concentration of 0.01 *wt*.%, precipitates were only a few hundred nanometers in diameter (Figure 3 (c) and Figure 4 (a_5)). On the other hand, a ten-fold concentration was needed to achieve similar precipitate sizes for XG and MC, and imbedding particles grew visibly larger as concentration decreased.

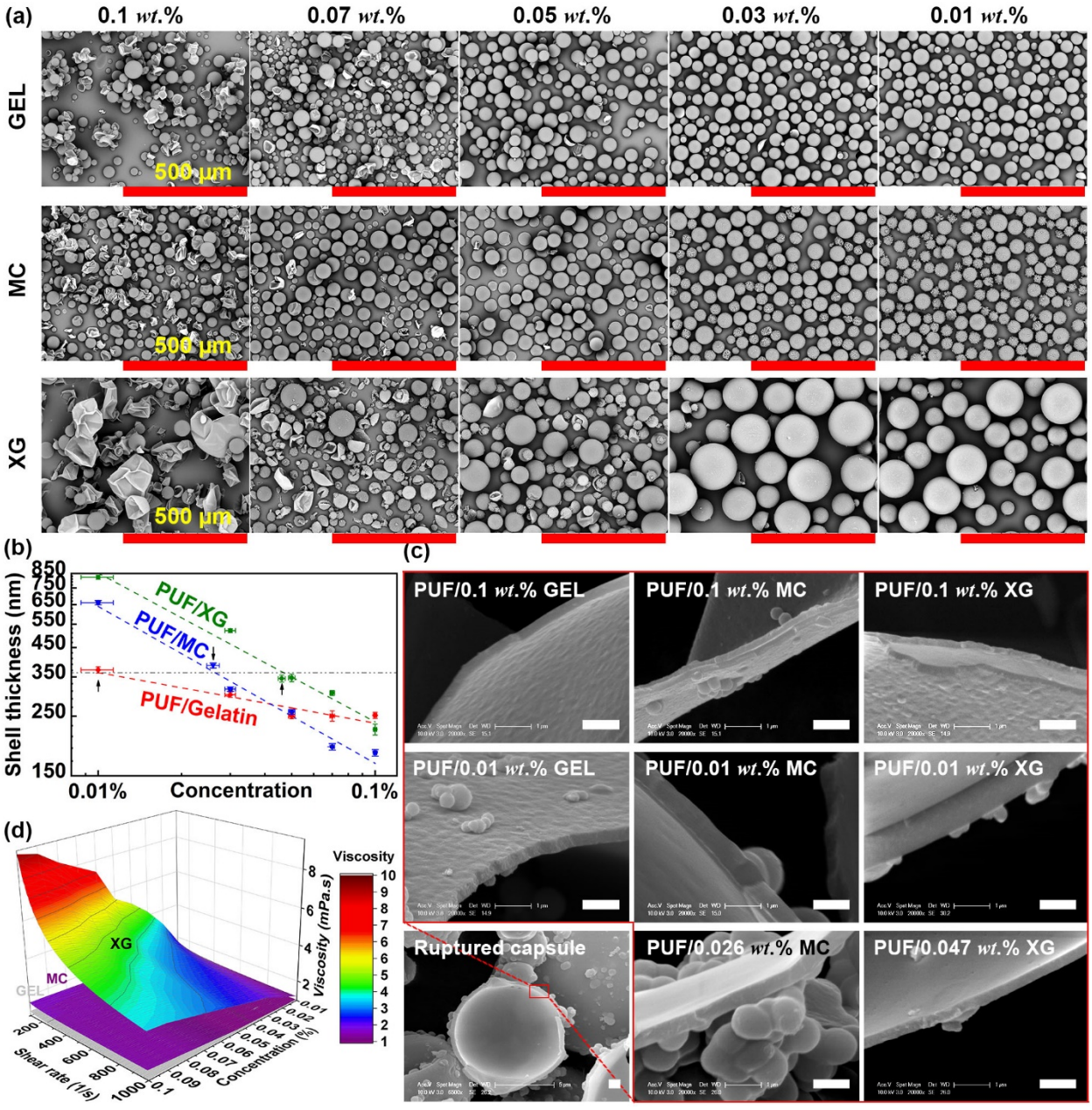

Figure 3 (a) Morphology of capsules synthesized with various concentrations of GEL, MC and XG; (b) effect of hydrocolloid concentration on shell thickness; (c) shell cross sections of ruptured capsules at miscellaneous hydrocolloid concentrations (all scale bars 1 μm); (d) bulk shear viscosity of hydrocolloid solutions as a functional of shear rate and hydrocolloid concentration.

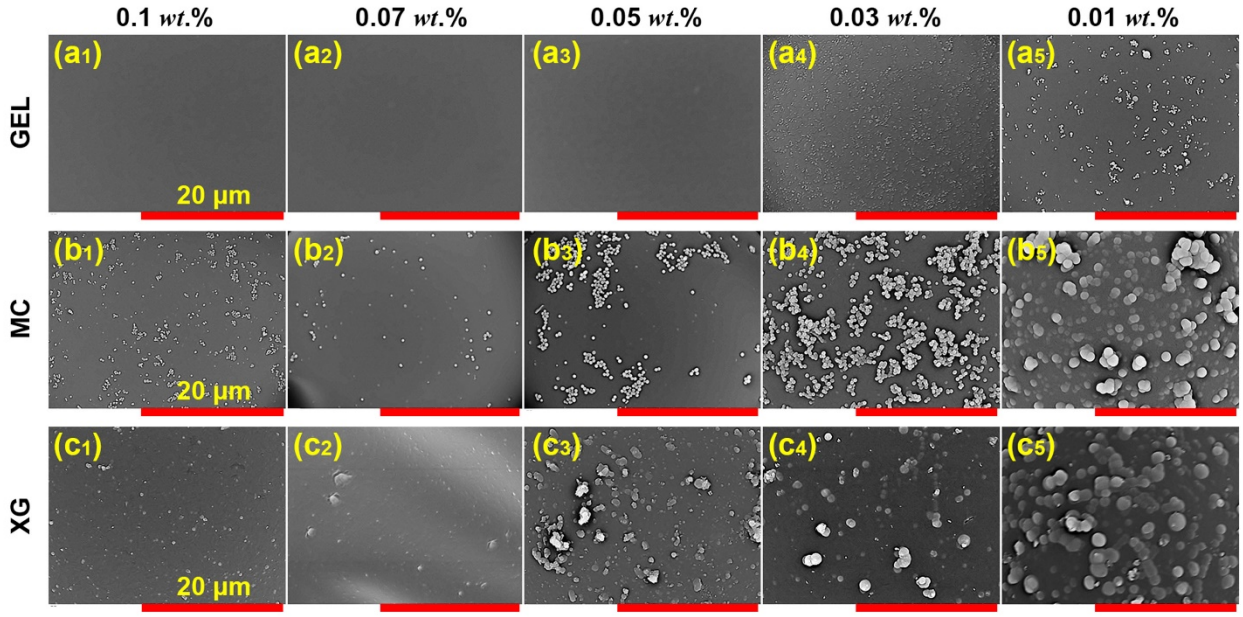

Figure 4 Surface morphology of capsules synthesized with GEL, MC and XG at miscellaneous concentrations as the emulsifier highlighting the size evolution of imbedding particles within shell structures (all scale bars 20 μm).

3.4. Micromanipulation – Mechanical compression

Microcapsules were tested by micromanipulation[89] as demonstrated in Figure 5 (a), and results disclosed that mechanical properties for capsules of similar shell thicknesses were comparable (Figure 5 (b)). Young's modulus was principally within 10 ~ 40 MPa with smaller capsules rising sharply to 60 ~ 100 MPa. Most capsules fractured around a 20% nominal strain with a typical rupture stress within 0.5 ~ 1.5 MPa. All loading curves resembled Figure 5 (c) (left) with a distinguishable ultimate failure. Broken capsules erupted the volatile heptane followed by rapid collapsing. Further compression transformed them into thin discs (Figure 5 (a)).

We noticed a remarkably diminishing percentage of capsules undergoing brittle failure with increasing hydrocolloid concentration (fracture proportion in Table 2 and Figure S4), shifting the loading characteristic to plastic deformation (Figure 5 (c) right). Capsules may have yielded and developed fine crazes during compression (Figure S5), but less abrupt ultimate failure was observed at higher hydrocolloid concentrations. Squashed capsules still had remaining heptane

after compression judging by the different light transmission in the live view (Figure 5 (c) right inset). Even for those that did show an ultimate failure, the rupture strain creeped up as manifested in a higher mean presented in Figure 5 (d). This could be a second implication that thin shells impart flexibility.

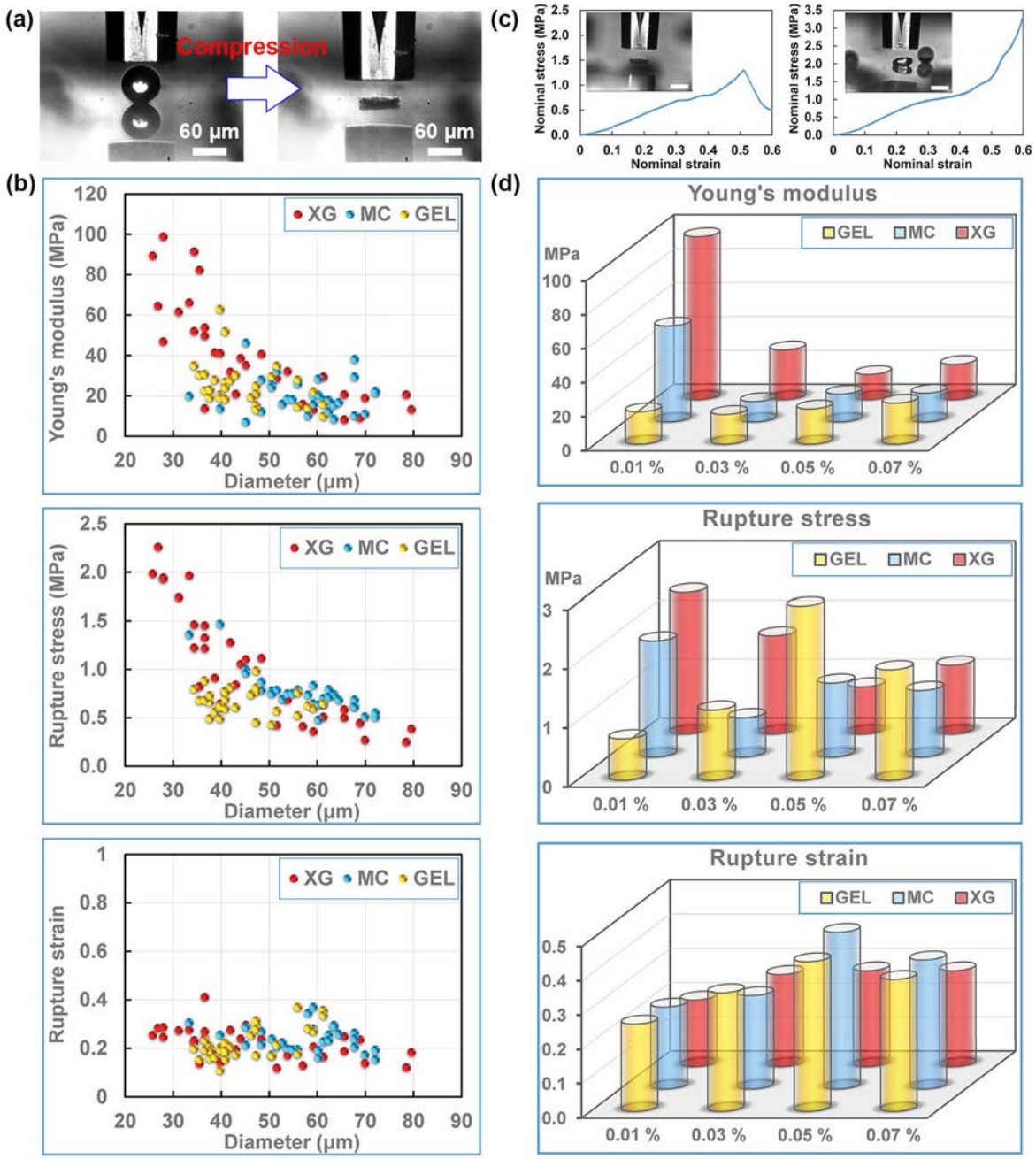

Figure 5 (a) Illustration of capsule compression by micromanipulation; (b) Young's modulus, nominal rupture stress and strain of capsules with similar shell thicknesses synthesized by 0.047 *wt.*% XG, 0.026 *wt.*%

MC and 0.01 *wt.*% GEL. A total number of 30 capsules were compressed for each sample; (c) loading curves corresponding to an abruptly ruptured capsule releasing volatile heptane and a plastically deformed capsule with residual heptane (inset image scale bars 60 μm); (d) the mean of Young's modulus, nominal rupture stress and strain of capsules formed by GEL, MC and XG at miscellaneous concentrations as tabulated in Table 2.

Table 2 Fracture ratio, Young's modulus, nominal rupture stress and strain of capsules produced by miscellaneous hydrocolloids of different concentrations

Hydrocolloid	Concentration (*wt.*%)	Shell thickness (nm)	Fracture proportion [a)]	Young's modulus [b)] (MPa)	Nominal rupture stress [c)] (MPa)	Nominal rupture strain [c)]
XG	0.01	823 ± 15	100 %	96.2 ± 11.7	2.4 ± 0.2	19 ± 2 %
	0.03	521 ± 8	93 %	29.4 ± 5.8	1.7 ± 0.7	27 ± 3 %
	0.05	347 ± 11	95 %	14.9 ± 2.6	0.8 ± 0.1	28 ± 2 %
	0.07	305 ± 6	74 %	20.8 ± 4.0	1.2 ± 0.2	28 ± 3 %
MC	0.01	662 ± 12	100 %	56.5 ± 9.1	2.0 ± 0.3	24 ± 3 %
	0.03	315 ± 6	100 %	11.9 ± 1.9	0.7 ± 0.1	27 ± 3 %
	0.05	259 ± 6	83 %	16.3 ± 3.1	1.3 ± 0.1	46 ± 4 %
	0.07	192 ± 5	13 %	16.2 ± 3.4	1.1 ± 0.7	38 ± 16 %
GEL	0.01	371 ± 10	92 %	18.9 ± 2.8	0.7 ± 0.1	25 ± 3 %
	0.03	301 ± 7	67 %	17.4 ± 2.1	1.2 ± 0.1	35 ± 4 %
	0.05	250 ± 5	38 %	20.6 ± 3.3	2.9 ± 1.5	44 ± 8 %
	0.07	251 ± 11	33 %	24.1 ± 4.9	1.9 ± 1.1	39 ± 6 %

[a)] A total number of 60 randomly selected capsules were compressed for each sample; [b)] the Young's modulus mean was calculated with all 60 capsules compressed for each sample. Microcapsules were assumed to be incompressible with a Poisson's ratio v=0.5; [c)] the nominal rupture stress and strain means were calculated among all capsules undergoing clear ultimate rupture failure.

Capsule Young's modulus for 0.01 *wt.*% XG and MC was significantly higher than those synthesized at higher concentrations or by GEL. For other concentrations, it was more or less on a similar level. The rough surfaces comprising protruding microscale PUF particles imbedded in shells (Figure 4) likely account for the enormously higher Young's modulus of the capsule (E_c). Since the Hertz equation for circular point contacts used to calculate Young's modulus of a capsule,

$$F = \frac{4E_c\sqrt{R}}{3(1-v^2)}\delta^{1.5} \quad (1)$$

, where F is compression force, E_c is the Young's modulus of the capsule, R is capsule radius, v is Poisson's ratio, δ is half of the total axial compression displacement, only applies to a minute

strain < 10%.[90-91], rough surfaces with imbedding particles would account for a large contribution to the strain range used for Young's modulus calculation.

3.5. Static leakage – Shell permeability

We tested core leakage with capsules of similar shell thicknesses produced by the three hydrocolloids at concentrations as indicated by the arrows in Figure 3 (b). The long-term leakage investigation was accomplished by comparing the difference in payload between as-formulated capsules and 30 days afterwards, which is presented in Figure 6. It clearly indicates very low leakage over 30 days and further calculation revealed weight losses for all samples were less than 10 *wt*.% . We have confirmed the mechanical stability of capsules with optical and electron microscopy. There is sufficient ground to assume that the leakage under static testing conditions at a nearly constant temperature is ascribed to the permeability of capsule shells, which is fundamentally of a solution-diffusion mechanism.[88] This is essentially distinct from the accelerated leakage under cyclic conditions to be discussed.

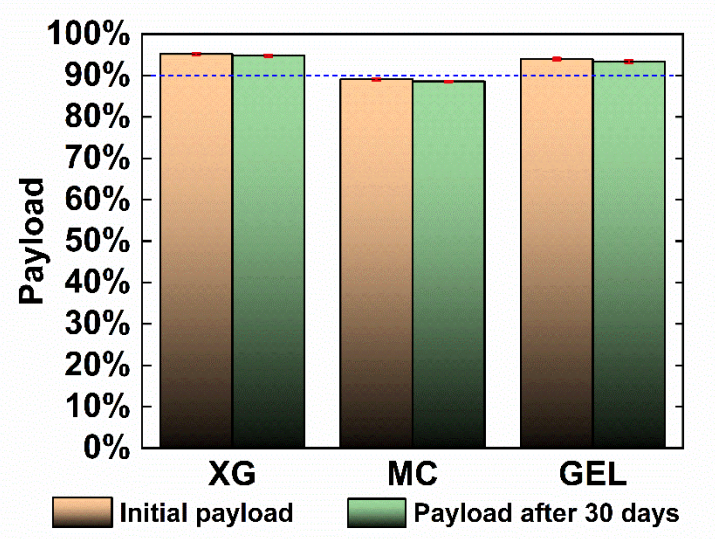

Figure 6 Payload of capsules produced by 0.047 *wt.*% XG, 0.026 *wt.*% MC and 0.01 *wt.*% GEL when freshly dried out of water and in the dry powder form after 30 days of climatization at 22 ± 2 ºC.

3.6. Accelerated leakage – Shell fatigue cracking

Micromanipulation quantified the mechanical properties of capsules from a non-cyclic perspective, but can be time-consuming to characterize the fatigue resistance of capsules under thermal cycling conditions. Dynamic conditions can jeopardize capsule integrity prominently and accelerate the leakage via fatigue structural defects. In order to test their cycling performance, we subjected miscellaneous capsules to 10 thermal cycles between 20 ºC and -140 ºC and compared their leakage under fluorescent microscopy as shown in Figure 7 (a) and (b). Figure 7 (c) presents the recorded cycling temperature profile and Figure 7 (d) confirmed the phase transition of pure and encapsulated cryoPCM heptane within this temperature range.

The shape integrity and bright green fluorescent color indicated that GEL helped capsules survive the cycling. Capsules formed with 0.01 *wt*.% MC underwent a severe loss of heptane as indicated by more than half of them losing the initial highly fluorescent green color. Even for those still exhibiting a bright green color, there were dark spots residing within the green regions, corresponding to air bubbles on account of heptane leakage. With MC concentration rising to 0.07 *wt*.%, fatigue resistance seemed to have improved substantially despite their thinner shells (Figure 3 (b)). 0.01 *wt*.% XG produced inferior capsules of leakage similar to MC. Increasing XG concentration, on the other hand, did not obtain distinguishing results with most capsules still losing their highly fluorescent green color after cycling.

The static leakage arising from shell permeability would not have lost the cryoPCM to the extent of dimming the highly fluorescent green color within the experimental time scale (< 12 h), as confirmed by Figure 2 (b) (after 24 h). Low temperatures would have further alleviated the leakage ascribing to less contribution from diffusion to the permeability coefficient owing to low kinetic energy of molecules,[92] if capsules had been intact. Thermal cycling, therefore, must have accelerated heptane release through shell cracking in capsules exhibiting severe leakage. SEM

micrographs in Figure 7 (e) clearly captured the fatigue cracks dwelling in shells mostly following the contours of imbedding PUF particles.

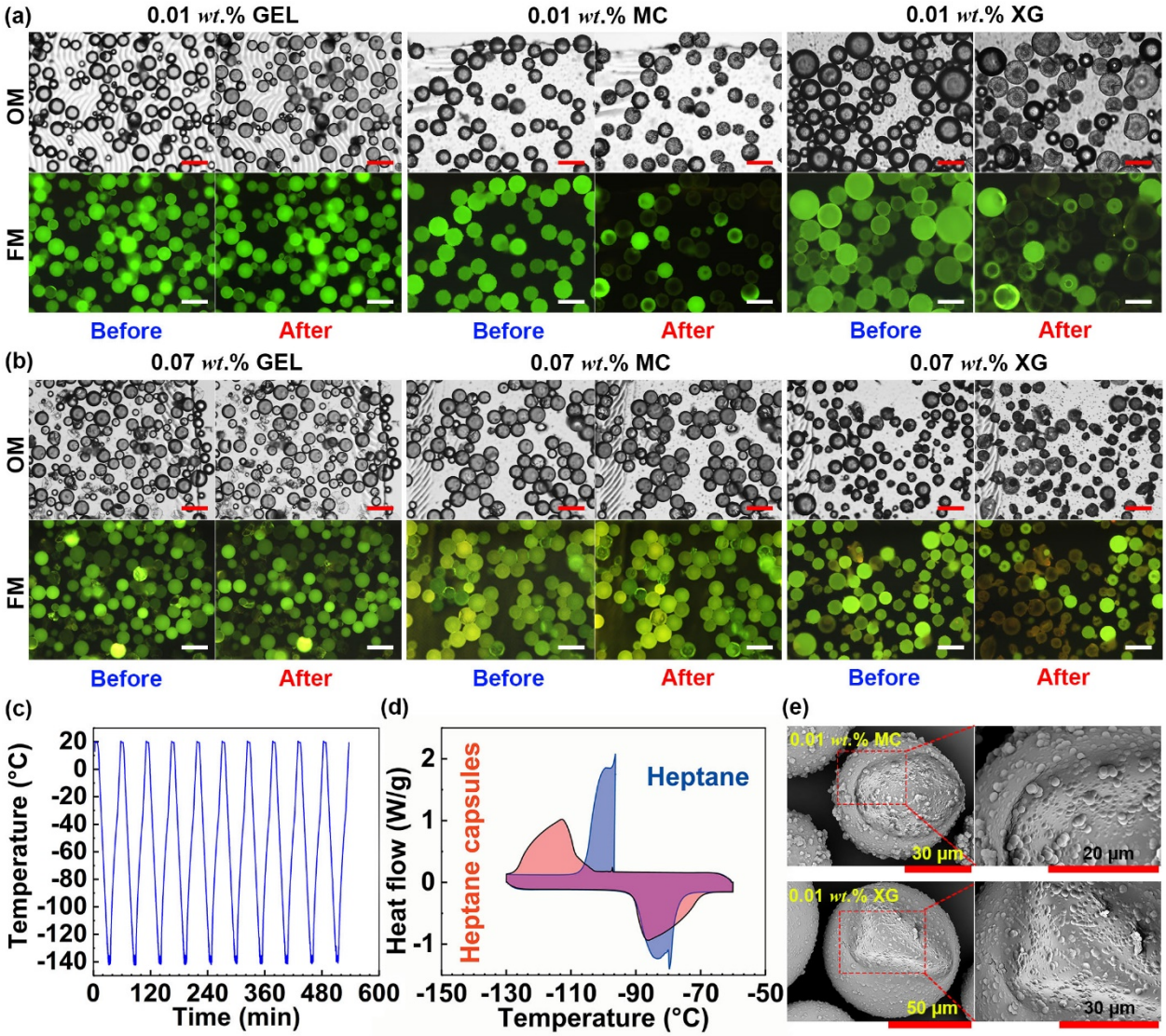

Figure 7 In situ comparison between capsules before and after thermal cycling formed with (a) 0.01 *wt.*% and (b) 0.07 wt.% GEL, MC and XG (all scale bars 100 μm) with fluorescent staining; (c) thermal cycling temperature profile: 5 min dwelling time at 20/-140 °C, heating/cooling rate 7.5 °C/min. Cooling was assisted by liquid nitrogen; (d) DSC thermogram of non-encapsulated heptane and heptane-PUF microcapsules produced by 0.01 *wt.*% GEL; (e) crack development and propogation along the buckling circumference after thermal cycling in capsule shells.

An inner cavity would appear coinciding with the volume change ascribable to a reducing heptane molecular spacing upon its crystallization.[93-94] Figure 8 (e) reminds us that it actually

existed prior to the phase transition. The elevated synthesis temperature at 55 ºC contributed to this as a consequence of the volumetric thermal expansion of liquid heptane. The density of heptane within 182.6 ~ 540.2 K can be estimated by the following equation: [95]

$$\rho(T) = C_1/C_2^{[1+(1-T/C_3)^{C_4}]} \quad (5)$$

where $\rho(T)$ is the density, T is temperature in Kelvin, C_1-C_4 are fitting constants. A temperature drop alone from 55 ºC to 25 ºC after synthesis ceases would induce a volume change ΔV around 4 *vol*.%. Buckling of polygonal shapes losing axisymmetry [96] has already been observed after synthesis at room temperature in both in Figure 8 (e) and previously.[56] A further 10 *vol*.% change enlarges the cavity to approximately 15 *vol*.% of the initial capsule volume (Figure S6) when temperature decreases from 25 ºC to -90 ºC before phase transition even occurs, which promotes capsule buckling.

For an ideal non-permeable capsule with a sufficiently strong and rigid shell filled up with liquid heptane, capsules could endure indefinite thermal cycles, transforming between (a) and (b) as shown in Figure 8 upon phase transition. In the case of a strong non-permeable non-rigid shell, repeated cycling would inflict frequent buckling-restoration on capsules as sketched in Figure 8 (a) and (c). Thin shells in practice, even though capable of tolerating such cycles as demonstrated in Figure 8 (e), are susceptible to both concave bending in response to an internal pressure decline and structural failure when the induced stress exceeds its yield strength.

Polymers normally yield via either low-energy crazing or high-energy ductile shear flow.[97] Even though flexibility improved with thin films as opposed to their bulk counterparts, the intrinsic thermosetting glassy nature of highly cross-linked amino resins remained unchanged. This made rearranging the molecular configuration or their movement with respect to one another in

response to external stress difficult.[98-99] We therefore postulate a crazing mechanism principally for PUF shell fatigue failure. Intermittent capsule buckling impinging along the circumference of the deflection dimples inflicted oscillating high concentration of stress within the folding region. This promoted fibril incubation where polymer chains were inclined to align in the molecular scale. Owing to its glassy nature, plastic deformation could not easily dissipate the excess energy. Accumulation of excessive energy eventually exceeded polymer cohesion and initiated permanent cracks locally. SEM revealed these defects in Figure 7 (e) at buckling borderlines. In a molecular rationale, intermolecular van der Waals forces between polymer chains were initially interrupted, followed by ultimate rupture of intramolecular covalent bonds in the backbone with continuous stress build-up. The propagation of cracks via their cumulative generation and coalescence after initiation was believed to be stress-induced chain scission, rather than heat-related scission or hysteresis considering the testing temperatures and loading frequency.

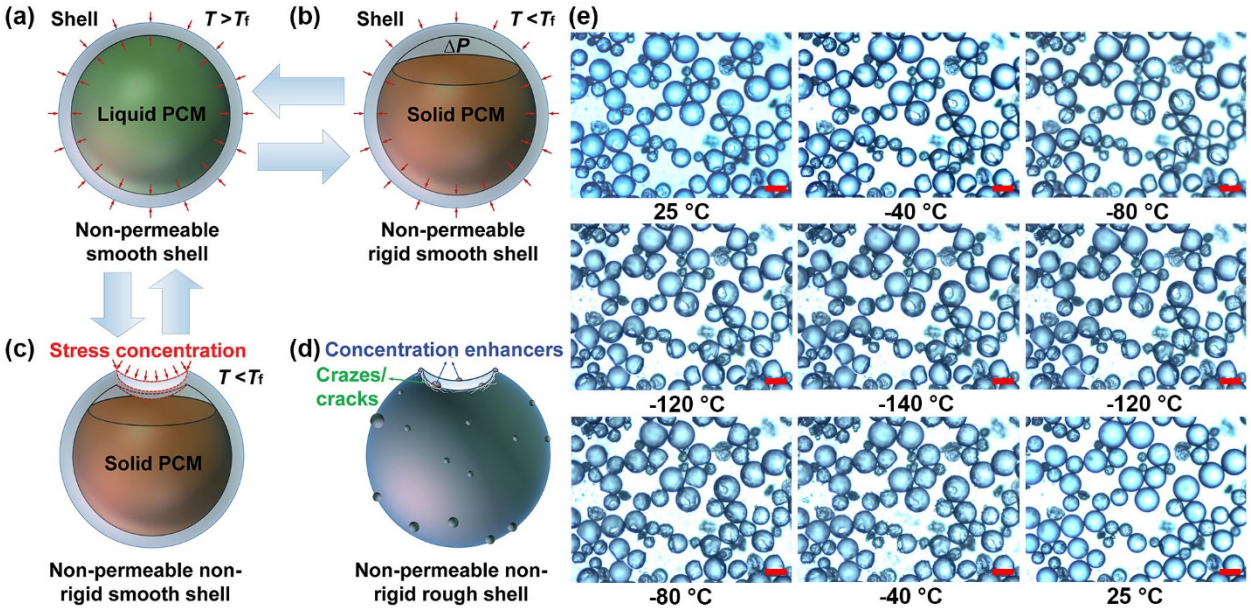

Figure 8 Shell indentation and capsule buckling during temperature change (sketches were not drawn to scale and are for illustration purpose only): (a) liquid PCM above its freeze point ($T>T_f$) occupies the full capacity of a capsule bearing an ideal non-permeable smooth shell; (b) solid PCM below its freeze point ($T<T_f$) occupies merely part of capsule capacity bearing an ideal non-permeable non-bendable smooth shell; (c) shell indentation on a non-permeable bendable smooth shell with stress concentration residing at the dotted deflection borderlines in red. An asymmetric simply buckled capsule is used for illustration purpose

here and the number of bulges as buckled (1~2 bulges) or crumpled (>2 bulges) may vary in pratice; (d) initiation and propagation of cracks from the deflection borderline with imbedding PUF particles acting as stress cocnentration enhancers for a non-permeable non-rigid rough shell; (e) obsevation of heptane-PUF capsule (0.01 *wt.*% GEL) deformation-restoration during one thermal cycle from 25 ºC to -140 ºC and back to 25 ºC under optical microscopy (scale bars 50 µm) within a cooling chamber (see the video in Supporting Information).

Lodging PUF particles inside shells added an additional source of stress concentration and further deteriorated the situation. The more PUF particles there were and the larger they were, the more likely they would be included within the buckling folding region. These stress concentration enhancers accelerated crack propagation via generation and coalescence of more crazes (Figure 8 (d)), compromising shell impermeability. These imbedding PUF particles, along with shell thickness, seemed to correlate with the cycling results presented in Figure 7. The cycling performance of capsules produced by MC improved significantly with thinner shells, as well as a reduction in size and the number of imbedding PUF particles. GEL, on the other hand, produced the most fatigue-resistant capsules at both low (0.01 *wt*.%) and high (0.07 *wt*.%) concentrations. This was in agreement with the observation that all capsules formed with GEL as the emulsifier had relatively thin shells with smooth surfaces. Imbedding particles were much smaller predominately in the submicron scale at low concentrations, while rarely seen at concentrations $\geq$ 0.05 *wt*.%. Taking the payload, encapsulation efficiency and cycling performance into consideration, GEL is regarded as an excellent emulsifier candidate for retaining cryoPCM via the one-step in situ polymerization and impart fatigue resistance among those tested.

3.7. CryoPCM retention – Why are hydrocolloids better?

The exact mechanism of shell formation after introducing hydrocolloids into the process is profoundly convoluted and more work is required for a mechanistic interpretation. Urea formaldehyde (UF) polycondensation, however, undoubtedly determines shell formation. Even

though carboxyl or anhydride moieties are not compulsory, any functional groups capable of modulating the principal polycondensation reactions at an appropriate rate within the formulation timescale could contribute to a dense shell structure. Slow reactions produce either weak shells or no capsules at all. Too fast, particle fusion owing to the Pickering emulsion effect dominates shell formation over homogenous molecular cross-linking, increasing shell permeability. Figure 9 (a) illustrates our proposed hydrocolloid-assisted shell formation. The advantages of hydrocolloids in improved shell impermeability likely underlie their modulation on the reaction rate from several aspects.

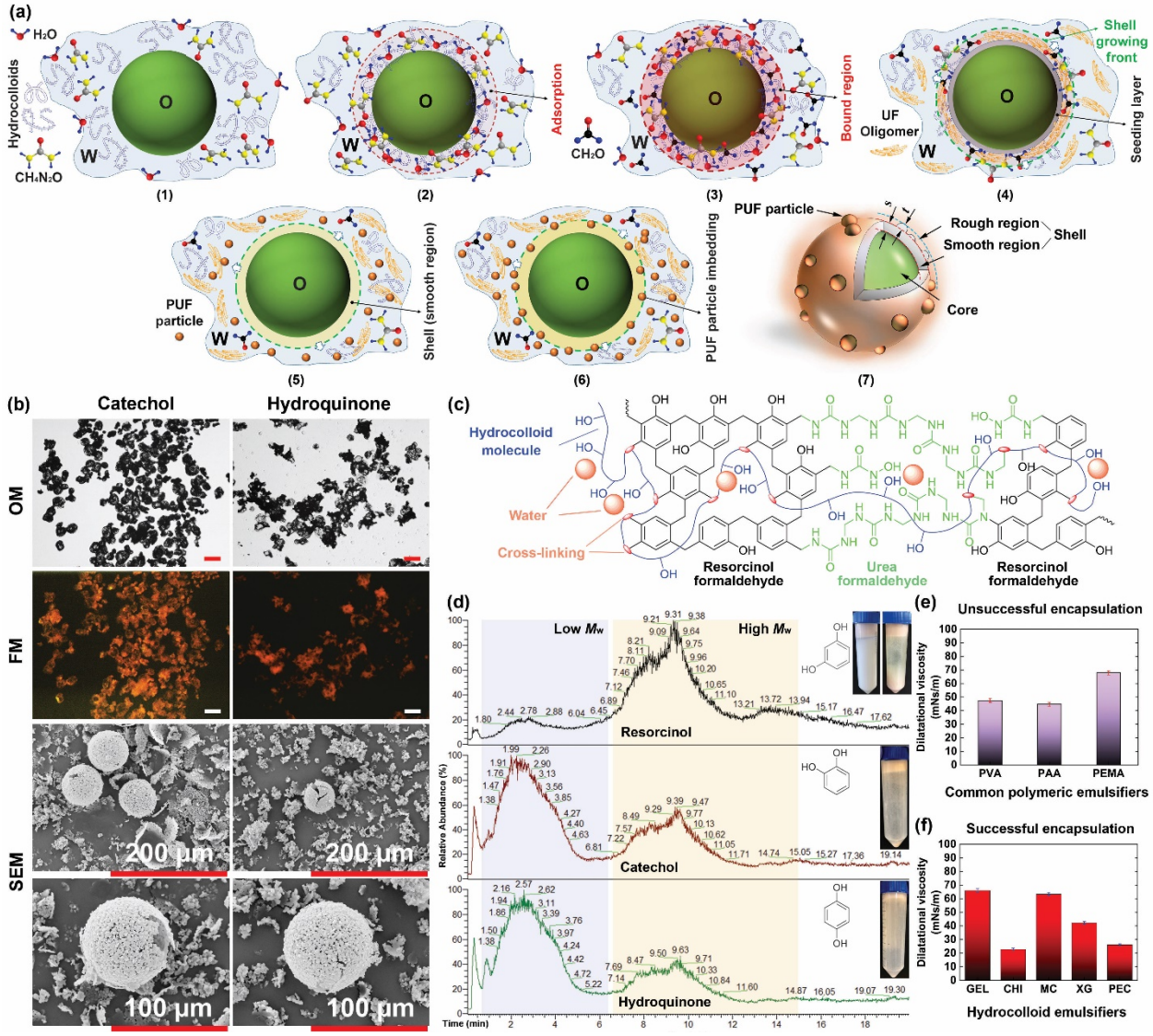

Figure 9 (a) Schematic illustration of encapsulation with the one-step in situ polymerization method using hydrocolloid emulsifers: (1) an O/W emulsion with all materials dissolved in water except formaldehyde; (2) adsorption of hydrocolloids at O/W interface binding other solutes; (3) adding formaldehyde; (4) producing PUF oligomers in both the interfacial region and the bulk continuous phase after pH adjustment and heat initiation; (5) formation of smooth shell region at O/W interface and precipitation of PUF particles in the bulk continuous phase; (6) continuous smooth shell region growth from oligomers and PUF particles imbedding in shell; (7) illustration a heptane-PUF microcapsule structure comprising imbedding particles within a layer of smooth PUF film; (b) OM, FM (scale bars 100 μm) and SEM micrographs of capsules produced with resorcinol alternatives – catechol and hydroquinone – showing their poor quality and the importance of resorcinol; (c) an illustrative sketch of the polymer structure comprising urea, resorcinol, hydrocolloids and formaldehyde (sketch is for illustration only and does not represent the true structure). The bonding between hydrocolloid molecules and PUF is represented by ovoids; (d) Electrospray ionization mass spectrometry (ESI-MS) analysis of the supertanants produced with resorcinol, catechol and hydroquinone clearly presenting the different retention times of the most abudant species and the turbodity appearance (insets). Longer retention time correpsonds to large molecules with low mobility. Supertanants for resorcinol are shown both before and afer centrifugation, while only those before centrifugation are presented for catechol and hydroquinone; dilatational viscosity of (e) common polymeric and (f) hydrocolloid emulsifiers at heptane/water interface (no chemical reaction initiation).

Firstly, the superior capability of hydrocolloids in viscosity enhancement of the aqueous reaction medium can inhibit polycondensation from proceeding too fast by reducing the diffusion rates and collision probability of reactants according to the simplified Smoluchowski and Stokes-Einstein equations.[107-108] However, previous bulk viscosity study did not seem to support such a claim,[65] and investigation in the continuous phase (Figure 2 (e) and Figure 3 (d)) divulged no significant viscosity change for most hydrocolloids at tested concentrations except for XG. One could argue that since in situ polymerization occurs at the O/W interface, interfacial other than bulk rheology would be more relevant. Nevertheless, Figure 9 (e) and (f) reveal no correlation between the interfacial viscosity and good retention either. Viscosity effect does not seem to be the principal cause for better retention. It must be noted, however, that rheology dynamics upon reaction initiation should be investigated ideally to obtain conclusive results. We only tested pristine emulsifier solutions without initiating chemical reactions.

Secondly, hydrocolloids are recognized for their strong water and solute binding abilities via hydrogen bonding (−OH···H) from the abundant hydroxyls in their molecules.[89-94] Hydrogen bonding strengthens anchoring monomers and subsequently form oligomers. This could produce

an interpenetrating hydrocolloid/monomer/oligomer network at the O/W interface through the adsorption of the hydrocolloid emulsifiers (or increasing accumulation near the oil phase in the case of non-adsorbing XG). Cross-linking the intercalated network results in a denser seeding layer than without hydrocolloids, which extends the growth of a less permeable polymer network into the aqueous phase through further intercalation and cross-linking. Unreacted polar moieties such as hydroxyls imparted into shells could also facilitate repelling nonpolar cargos by reducing its coefficient of diffusion through the shell via enlarging the discrepancy in the core-shell hydrogen bonding components (δ_h) of their Hansen solubility parameters (HSP).[95]

Mostly importantly, miscellaneous additional chemical reactions, characteristic of hydrocolloids, may have modified the system rheology, changed the PUF growth kinetics, and increased cross-linking density for enhanced barrier property. Polysaccharides can undergo acidic hydrolysis and convert hydroxyls into aldehydes,[79-83] promoting reactions with urea, and have also been reported to react with phenols and alcohols.[84-87] Amine groups on GEL and CHI molecules, akin to those from melamine, can also react with formaldehyde. Reaction between UF oligomers and gelatin via amine and hydroxyl moieties has been proposed.[88]

We have demonstrated the advantages of hydrocolloids over common polymeric emulsifiers in Figure 1 (b)-(d) and Figure 2 (b). We now approve that specific reactions between hydrocolloids and resorcinol are the key to successful cryoPCM retention with the one-step in situ polymerization. We replaced the cross-linker resorcinol with the ortho- (catechol) and para- (hydroquinone) isomers of dihydroxybenzenes at the presence of gelatin – the best hydrocolloid emulsifier tested. Neither of the alternatives yielded comparable retention with most capsules not forming at all but only broken pieces (Figure 9 (b)). This suggest that polymerization may have proceeded at a much slower rate which hindered capsule formation. Electrospray ionization mass

spectrometry (ESI-MS) analysis (Figure 9 (d)) of the supernatants after harvesting capsules following centrifugation provided some preliminary evidence for such an argument. The most abundant species in the supernatant when using resorcinol appeared to have longer retention times (9~10 min) correponding to higher molecular weights. However, with both catechol and hydroquinone, this shifted to a shorter retention time range (< 3 min) corresponding to lower molecular weights. Another evidence is that when using resorcinol, the supertanant after synthesis was very cloudy and milky before centrifugation but became clearer afterwards (Figure 9 (d) insets) due to sendimentation. For samples produced with catechol and hydroquinone, the supernatants were rather clear even before centrifugation (Figure 9 (d) insets) and not much sendimentation was observed.

The unique physical and chemical properties of hydrocolloids facilitated them in modulating the principal polycondensation reactions, leading to less permeable polymer structures (Figure 9 (c)). If so, any emulsifiers capable of such modulation, theoretically, should qualify as suitable candidates. Our results suggest that reactions are generally too fast with carboxyls, while too slow with hydroxyls. We, therefore, tested amines and amides on the grounds that these are the functional moeities in the reactions of amino resin families and can contribute to the principal polycondensation reactions at a comparable rate. Both polyacrylamide and polyethylenimine were successful in retaining heptane as indicated by the green fluorescent color in Figure 10. Payload after 24 h drying was quantified to be 92±1 *wt*.% and 93±2 wt.%, respectively.

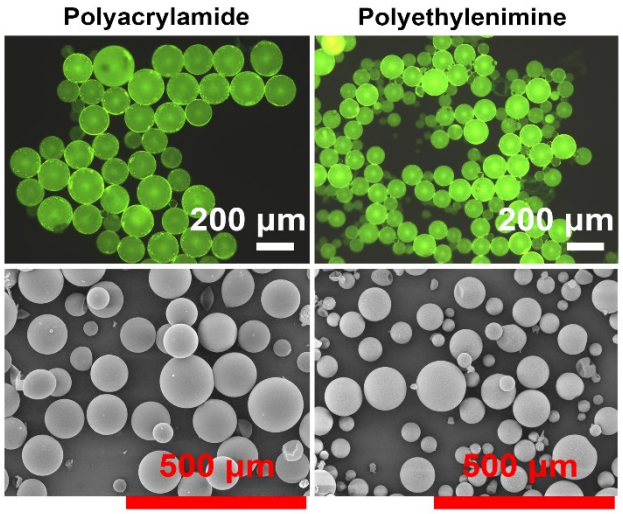

Figure 10 FM and SEM micrographs of dry capsules (24 h) produced by 0.03 *wt.*% polyacrylamide and polyethylenimine as emulsifiers.

4. Conclusions

In this work, we reported a family of emulsifiers, known as hydrocolloids, for their indispensable role in the containment of volatile cryoPCM within amino resin capsules. These molecules, possessing a wide range of anomalous features such as carrying identical charges with the shell polymer precipitates, lacking certain functional moieties postulated to be necessary for chemical reactions, or bearing low surface activities, defied common beliefs and proved to be constructive to encapsulation via the one-step in situ polymerization. The volatile cryoPCM heptane, not effectively retained by common polymeric emulsifiers, was successfully sealed inside high payload capsules under the assistance of these hydrocolloids. The significance of our findings underlies in that the broadened emulsifier range enables fine-tuning capsule size, shell thickness, mechanical and barrier properties, as well as surface roughness for different applications. The high payloads, high core-shell volume ratio and thin shells achieved enable such capsules to qualify for cryogenic energy transport and storage. Using gelatin as an emulsifier can eliminate

the commonly encountered imbedding particles in the shell structure to achieve extremely smooth surfaces ever achieved with the one-step route. Direct observation of capsule buckling at low temperatures and restoration at room temperature provides evidence for their thermal stability. Such findings not only enable in situ polymerization to match other synthesis routes in smooth surfaced capsule fabrication when light transmission is critical, but also contribute to the obliteration of additional stress concentrators from the shell upon thermal cycling for improved fatigue resistance in our cryogenic energy storage and transport application. We proposed that the unique physical and chemical properties of hydrocolloids facilitate in modulating the main polycondensation reactions so that less permeable shells could be produced. Under such a premise, two non-hydrocolloid polymeric emulsifiers were identified and tested successful for cryoPCM encapsulation, providing evidence that modulating the main polycondensation reactions is essential for emulsifiers to successfully seal volatile cryoPCM with one-step in situ polymerization.

Acknowledgements

The authors express their sincere gratitude to the Engineering and Physical Sciences Research Council (EPSRC) for the funding provided to this project (EP/N000714/1 and EP/N021142/1). Special thanks are given to Dr Chi Tsang from School of Chemistry at University of Birmingham for his contribution to the electrospray ionization mass spectrometry. The authors also express their gratitude for Ms. Jie Chen and Mr. Gan Zhang from Birmingham Centre for Energy Storage (BCES) in the School of Chemical Engineering at University of Birmingham for their generous support in this work. Yan Zhang designed all experiments and performed bright-field, fluorescence and electron microcopy characterization, electrophoresis mobility tests, interfacial tension measurement, FTIR, payload characterization, leakage tests and thermal

cycling and most capsule synthesis, analyzed experimental data, and drafted the manuscript unless specified otherwise. Daniele Baiocco completed most micromanipulation tests and compression data analysis, with partial contribution from Xiaotong Zhang and Yan Zhang. Abdullah Mustapha carried out all bulk and interfacial rheology study, produced capsules with poly(ethylene-alt-maleic anhydride) and resorcinol alternatives, as well as sample characterization by microscopy. Qinghua Yu contributed in part to drafting the introduction of this manuscript. Gilmore Wellio contributed in part to the Linkam stage bright-field microscopy experiment. Zhibing Zhang and Yongliang Li supervised and complemented the project with suggestions. All authors made comments on the manuscript.

References

(1) White, A.; Parks, G.; Markides, C. N., Thermodynamic Analysis of Pumped Thermal Electricity Storage. *Applied Thermal Engineering* **2013,** *53* (2), 291-298.
(2) Morgan, R.; Nelmes, S.; Gibson, E.; Brett, G., Liquid Air Energy Storage – Analysis and First Results from a Pilot Scale Demonstration Plant. *Applied Energy* **2015,** *137*, 845-853.
(3) She, X.; Peng, X.; Nie, B.; Leng, G.; Zhang, X.; Weng, L.; Tong, L.; Zheng, L.; Wang, L.; Ding, Y., Enhancement of Round Trip Efficiency of Liquid Air Energy Storage through Effective Utilization of Heat of Compression. *Applied Energy* **2017,** *206*, 1632-1642.
(4) Li, Y.; Wang, X.; Ding, Y., An Optimal Design Methodology for Large-Scale Gas Liquefaction. *Applied Energy* **2012,** *99*, 484-490.
(5) Wang, M.; Xu, Q., Optimal Design and Operation for Simultaneous Shale Gas Ngl Recovery and Lng Re-Gasification under Uncertainties. *Chemical Engineering Science* **2014,** *112*, 130-142.
(6) Thess, A., Thermodynamic Efficiency of Pumped Heat Electricity Storage. *Physical Review Letters* **2013,** *111* (11), 110602.
(7) Guizzi, G. L.; Manno, M.; Tolomei, L. M.; Vitali, R. M., Thermodynamic Analysis of a Liquid Air Energy Storage System. *Energy* **2015,** *93*, 1639-1647.
(8) Peng, H.; Shan, X.; Yang, Y.; Ling, X., A Study on Performance of a Liquid Air Energy Storage System with Packed Bed Units. *Applied Energy* **2018,** *211*, 126-135.
(9) McTigue, J. D.; White, A. J.; Markides, C. N., Parametric Studies and Optimisation of Pumped Thermal Electricity Storage. *Applied Energy* **2015,** *137*, 800-811.
(10) Sciacovelli, A.; Vecchi, A.; Ding, Y., Liquid Air Energy Storage (Laes) with Packed Bed Cold Thermal Storage – from Component to System Level Performance through Dynamic Modelling. *Applied Energy* **2017,** *190*, 84-98.
(11) Chai, L.; Liu, J.; Wang, L.; Yue, L.; Yang, L.; Sheng, Y.; Chen, H.; Tan, C., Cryogenic Energy Storage Characteristics of a Packed Bed at Different Pressures. *Applied Thermal Engineering* **2014,** *63* (1), 439-446.

(12) Peng, H.; Yang, Y.; Li, R.; Ling, X., Thermodynamic Analysis of an Improved Adiabatic Compressed Air Energy Storage System. *Applied Energy* **2016,** *183*, 1361-1373.
(13) Ma, X.; Omer, S. A.; Riffat, S. B.; Zhang, W., Investigation of Energy Transportation Capability of a Phase Change Slurry through a Cold Storage-Cooling Coil System. *International Journal of Energy Research* **2009,** *33* (11), 999-1004.
(14) Horcajada, P.; Chalati, T.; Serre, C.; Gillet, B.; Sebrie, C.; Baati, T.; Eubank, J. F.; Heurtaux, D.; Clayette, P.; Kreuz, C.; Chang, J.-S.; Hwang, Y. K.; Marsaud, V.; Bories, P.-N.; Cynober, L.; Gil, S.; Férey, G.; Couvreur, P.; Gref, R., Porous Metal–Organic-Framework Nanoscale Carriers as a Potential Platform for Drug Delivery and Imaging. *Nature Materials* **2009,** *9*, 172.
(15) Zieringer, M. A.; Carroll, N. J.; Abbaspourrad, A.; Koehler, S. A.; Weitz, D. A., Microcapsules for Enhanced Cargo Retention and Diversity. *Small* **2015,** *11* (24), 2903-2909.
(16) Lomova, M. V.; Brichkina, A. I.; Kiryukhin, M. V.; Vasina, E. N.; Pavlov, A. M.; Gorin, D. A.; Sukhorukov, G. B.; Antipina, M. N., Multilayer Capsules of Bovine Serum Albumin and Tannic Acid for Controlled Release by Enzymatic Degradation. *ACS Applied Materials & Interfaces* **2015,** *7* (22), 11732-11740.
(17) Sadovoy, A. V.; Lomova, M. V.; Antipina, M. N.; Braun, N. A.; Sukhorukov, G. B.; Kiryukhin, M. V., Layer-by-Layer Assembled Multilayer Shells for Encapsulation and Release of Fragrance. *ACS Applied Materials & Interfaces* **2013,** *5* (18), 8948-8954.
(18) Lee, H.; Choi, C.-H.; Abbaspourrad, A.; Wesner, C.; Caggioni, M.; Zhu, T.; Weitz, D. A., Encapsulation and Enhanced Retention of Fragrance in Polymer Microcapsules. *ACS Applied Materials & Interfaces* **2016,** *8* (6), 4007-4013.
(19) Günay, K. A.; Berthier, D. L.; Jerri, H. A.; Benczédi, D.; Klok, H.-A.; Herrmann, A., Selective Peptide-Mediated Enhanced Deposition of Polymer Fragrance Delivery Systems on Human Hair. *ACS Applied Materials & Interfaces* **2017,** *9* (28), 24238-24249.
(20) Lv, L.-P.; Zhao, Y.; Vilbrandt, N.; Gallei, M.; Vimalanandan, A.; Rohwerder, M.; Landfester, K.; Crespy, D., Redox Responsive Release of Hydrophobic Self-Healing Agents from Polyaniline Capsules. *Journal of the American Chemical Society* **2013,** *135* (38), 14198-14205.
(21) Gao, L.; He, J.; Hu, J.; Wang, C., Photoresponsive Self-Healing Polymer Composite with Photoabsorbing Hybrid Microcapsules. *ACS Applied Materials & Interfaces* **2015,** *7* (45), 25546-25552.
(22) Tan, Y. J.; Wu, J.; Li, H.; Tee, B. C. K., Self-Healing Electronic Materials for a Smart and Sustainable Future. *ACS Applied Materials & Interfaces* **2018,** *10* (18), 15331-15345.
(23) Alford, A.; Kozlovskaya, V.; Xue, B.; Gupta, N.; Higgins, W.; Pham-Hua, D.; He, L.; Urban, V. S.; Tse, H. M.; Kharlampieva, E., Manganoporphyrin-Polyphenol Multilayer Capsules as Radical and Reactive Oxygen Species (Ros) Scavengers. *Chemistry of Materials* **2018,** *30* (2), 344-357.
(24) Baginska, M.; Blaiszik, B. J.; Merriman, R. J.; Sottos, N. R.; Moore, J. S.; White, S. R., Autonomic Shutdown of Lithium-Ion Batteries Using Thermoresponsive Microspheres. *Advanced Energy Materials* **2012,** *2* (5), 583-590.
(25) Wang, X.; Li, G.; Li, J.; Zhang, Y.; Wook, A.; Yu, A.; Chen, Z., Structural and Chemical Synergistic Encapsulation of Polysulfides Enables Ultralong-Life Lithium–Sulfur Batteries. *Energy & Environmental Science* **2016,** *9* (8), 2533-2538.

(26) Lim, T.-W.; Park, C. W.; White, S. R.; Sottos, N. R., Time Release of Encapsulated Additives for Enhanced Performance of Lithium-Ion Batteries. *ACS Applied Materials & Interfaces* **2017,** *9* (46), 40244-40251.
(27) Baginska, M.; Sottos, N. R.; White, S. R., Core–Shell Microcapsules Containing Flame Retardant Tris(2-Chloroethyl Phosphate) for Lithium-Ion Battery Applications. *ACS Omega* **2018,** *3* (2), 1609-1613.
(28) Tamaki, T.; Kuroki, H.; Ogura, S.; Fuchigami, T.; Kitamoto, Y.; Yamaguchi, T., Connected Nanoparticle Catalysts Possessing a Porous, Hollow Capsule Structure as Carbon-Free Electrocatalysts for Oxygen Reduction in Polymer Electrolyte Fuel Cells. *Energy & Environmental Science* **2015,** *8* (12), 3545-3549.
(29) Qi, G.; Wang, Y.; Estevez, L.; Duan, X.; Anako, N.; Park, A.-H. A.; Li, W.; Jones, C. W.; Giannelis, E. P., High Efficiency Nanocomposite Sorbents for Co2 Capture Based on Amine-Functionalized Mesoporous Capsules. *Energy & Environmental Science* **2011,** *4* (2), 444-452.
(30) Zheng, Z.; Jin, J.; Xu, G.-K.; Zou, J.; Wais, U.; Beckett, A.; Heil, T.; Higgins, S.; Guan, L.; Wang, Y.; Shchukin, D., Highly Stable and Conductive Microcapsules for Enhancement of Joule Heating Performance. *ACS Nano* **2016,** *10* (4), 4695-4703.
(31) Zheng, Z.; Chang, Z.; Xu, G.-K.; McBride, F.; Ho, A.; Zhuola, Z.; Michailidis, M.; Li, W.; Raval, R.; Akhtar, R.; Shchukin, D., Microencapsulated Phase Change Materials in Solar-Thermal Conversion Systems: Understanding Geometry-Dependent Heating Efficiency and System Reliability. *ACS Nano* **2017,** *11* (1), 721-729.
(32) Aftab, W.; Huang, X.; Wu, W.; Liang, Z.; Mahmood, A.; Zou, R., Nanoconfined Phase Change Materials for Thermal Energy Applications. *Energy & Environmental Science* **2018,** *11* (6), 1392-1424.
(33) Derwent, R. G., Sources, Distributions, and Fates of Vocs in the Atmosphere. In *Volatile Organic Compounds in the Atmosphere*, Hester, R. E.; Harrison, R. M., Eds. The Royal Society of Chemistry: Cambridge, U.K., 1995; pp 1-16.
(34) Scheithauer, M., Measurement and Estimation of Solvents Emission and Odor. In *Handbook of Solvents*, Wypych, G., Ed. ChemTec Publishing and William Andrew Publishing: Toronto, New York, 2001; pp 1201-1226.
(35) Butte, W.; Heinzow, B., Pollutants in Hourse Dust as Indicators of Indoor Contamination. In *Reviews of Environmental Contamination and Toxicology*, Ware, G. W., Ed. Springer: New York, USA, 2002; Vol. 175, pp 1-36.
(36) Patchan, M. W.; Baird, L. M.; Rhim, Y.-R.; LaBarre, E. D.; Maisano, A. J.; Deacon, R. M.; Xia, Z.; Benkoski, J. J., Liquid-Filled Metal Microcapsules. *ACS Applied Materials & Interfaces* **2012,** *4* (5), 2406-2412.
(37) Hitchcock, J. P.; Tasker, A. L.; Baxter, E. A.; Biggs, S.; Cayre, O. J., Long-Term Retention of Small, Volatile Molecular Species within Metallic Microcapsules. *ACS Applied Materials & Interfaces* **2015,** *7* (27), 14808-14815.
(38) Ibrahim, A. M.; Mahadevan, V.; Srinivasan, M., Low Glass Transition Temperature Aliphatic Polyurethanes. *Polymer Bulletin* **1980,** *3* (1), 97-101.
(39) Nabeth, B.; Corniglion, I.; Pascault, J. P., Influence of the Composition on the Glass Transition Temperature of Polyurethane and Polyurethane Acrylate Networks. *Journal of Polymer Science Part B: Polymer Physics* **1996,** *34* (3), 401-417.
(40) Chen, T. K.; Chui, J. Y.; Shieh, T. S., Glass Transition Behaviors of a Polyurethane Hard Segment Based on 4,4‘-Diisocyanatodiphenylmethane and 1,4-Butanediol and the Calculation of Microdomain Composition. *Macromolecules* **1997,** *30* (17), 5068-5074.

(41) Shanks, R. A.; Kong, I., General Purpose Elastomers: Structure, Chemistry, Physics and Performance. In *Advances in Elastomers I: Blends and Interpenetrating Networks*, Visakh, P. M.; Thomas, S.; Chandra, A. K.; Mathew, A. P., Eds. Springer Berlin Heidelberg: Berlin, Heidelberg, 2013; pp 11-45.
(42) Yoo, Y.; Martinez, C.; Youngblood, J. P., Synthesis and Characterization of Microencapsulated Phase Change Materials with Poly(Urea−Urethane) Shells Containing Cellulose Nanocrystals. *ACS Applied Materials & Interfaces* **2017,** *9* (37), 31763-31776.
(43) Lee, J. N.; Park, C.; Whitesides, G. M., Solvent Compatibility of Poly(Dimethylsiloxane)-Based Microfluidic Devices. *Analytical Chemistry* **2003,** *75* (23), 6544-6554.
(44) Ogieglo, W.; van der Werf, H.; Tempelman, K.; Wormeester, H.; Wessling, M.; Nijmeijer, A.; Benes, N. E., N-Hexane Induced Swelling of Thin Pdms Films under Non-Equilibrium Nanofiltration Permeation Conditions, Resolved by Spectroscopic Ellipsometry. *Journal of Membrane Science* **2013,** *431*, 233-243.
(45) Torza, S.; Mason, S. G., Coalescence of Two Immiscible Liquid Drops. *Science* **1969,** *163* (3869), 813-814.
(46) Loxley, A.; Vincent, B., Preparation of Poly(Methylmethacrylate) Microcapsules with Liquid Cores. *Journal of Colloid and Interface Science* **1998,** *208* (1), 49-62.
(47) González, L.; Kostrzewska, M.; Baoguang, M.; Li, L.; Hansen, J. H.; Hvilsted, S.; Skov, A. L., Preparation and Characterization of Silicone Liquid Core/Polymer Shell Microcapsules Via Internal Phase Separation. *Macromolecular Materials and Engineering* **2014,** *299* (10), 1259-1267.
(48) Fujiwara, M.; Shiokawa, K.; Tanaka, Y.; Nakahara, Y., Preparation and Formation Mechanism of Silica Microcapsules (Hollow Sphere) by Water/Oil/Water Interfacial Reaction. *Chemistry of Materials* **2004,** *16* (25), 5420-5426.
(49) Fang, G.; Chen, Z.; Li, H., Synthesis and Properties of Microencapsulated Paraffin Composites with Sio2 Shell as Thermal Energy Storage Materials. *Chemical Engineering Journal* **2010,** *163* (1–2), 154-159.
(50) Cao, Z.; Dong, L.; Li, L.; Shang, Y.; Qi, D.; Lv, Q.; Shan, G.; Ziener, U.; Landfester, K., Preparation of Mesoporous Submicrometer Silica Capsules Via an Interfacial Sol–Gel Process in Inverse Miniemulsion. *Langmuir* **2012,** *28* (17), 7023-7032.
(51) Zhang, L.; D'Acunzi, M.; Kappl, M.; Imhof, A.; Blaaderen, A. v.; Butt, H.-J.; Graf, R.; Vollmer, D., Tuning the Mechanical Properties of Silica Microcapsules. *Physical Chemistry Chemical Physics* **2010,** *12* (47), 15392-15398.
(52) Brown, E. N.; Kessler, M. R.; Sottos, N. R.; White, S. R., In Situ Poly(Urea-Formaldehyde) Microencapsulation of Dicyclopentadiene. *Journal of Microencapsulation* **2003,** *20* (6), 719-730.
(53) Yoshizawa, H.; Kamio, E.; Kobayashi, E.; Jacobson, J.; Kitamura, Y., Investigation of Alternative Compounds to Poly(E-Ma) as a Polymeric Surfactant for Preparation of Microcapsules by Phase Separation Method. *Journal of Microencapsulation* **2007,** *24* (4), 349-357.
(54) Fan, C.; Zhou, X., Effect of Emulsifier on Poly(Urea–Formaldehyde) Microencapsulation of Tetrachloroethylene. *Polymer Bulletin* **2011,** *67* (1), 15-27.
(55) Zhang, Y.; Zhang, Z.; Ding, Y.; Pikramenou, Z.; Li, Y., Converting Capsules to Sensors for Nondestructive Analysis: From Cargo-Responsive Self-Sensing to Functional Characterization. *ACS Applied Materials & Interfaces* **2019,** *11* (9), 8693-9642.

(56) Zhang, Y.; Jiang, Z.; Zhang, Z.; Ding, Y.; Yu, Q.; Li, Y., Polysaccharide Assisted Microencapsulation for Volatile Phase Change Materials with a Fluorescent Retention Indicator. *Chemical Engineering Journal* **2019,** *359*, 1234-1243.
(57) Wohlfarth, C., *Crc Handbook of Chemistry and Physics*. 85th ed.; CRC Press: Boca Raton, FL, USA, 2005.
(58) Katoueizadeh, E.; Zebarjad, S. M.; Janghorban, K., Investigating the Effect of Synthesis Conditions on the Formation of Urea–Formaldehyde Microcapsules. *Journal of Materials Research and Technology* **2018**.
(59) Brown, E. N.; White, S. R.; Sottos, N. R., Microcapsule Induced Toughening in a Self-Healing Polymer Composite. *Journal of Materials Science* **2004,** *39* (5), 1703-1710.
(60) Yoshizawa, H.; Kamio, E.; Hirabayashi, N.; Jacobson, J.; Kitamura, Y., Membrane Formation Mechanism of Cross-Linked Polyurea Microcapsules by Phase Separation Method. *Journal of Microencapsulation* **2004,** *21* (3), 241-249.
(61) Blaiszik, B. J.; Caruso, M. M.; McIlroy, D. A.; Moore, J. S.; White, S. R.; Sottos, N. R., Microcapsules Filled with Reactive Solutions for Self-Healing Materials. *Polymer* **2009,** *50* (4), 990-997.
(62) Fan, C.; Zhou, X., Influence of Operating Conditions on the Surface Morphology of Microcapsules Prepared by in Situ Polymerization. *Colloids and Surfaces A: Physicochemical and Engineering Aspects* **2010,** *363* (1), 49-55.
(63) Tang, J.; Fan, C.; Lin, Q.; Zhou, X., Smooth, Stable and Optically Transparent Microcapsules Prepared by One-Step Method Using Sodium Carboxymethyl Cellulose as Protective Colloid. *Colloids and Surfaces A: Physicochemical and Engineering Aspects* **2014,** *459* (Supplement C), 65-73.
(64) Fei, X.; Zhao, H.; Zhang, B.; Cao, L.; Yu, M.; Zhou, J.; Yu, L., Microencapsulation Mechanism and Size Control of Fragrance Microcapsules with Melamine Resin Shell. *Colloids and Surfaces A: Physicochemical and Engineering Aspects* **2015,** *469* (Supplement C), 300-306.
(65) Zeppieri, S.; Rodríguez, J.; López de Ramos, A. L., Interfacial Tension of Alkane + Water Systems. *Journal of Chemical & Engineering Data* **2001,** *46* (5), 1086-1088.
(66) Zhang, S.; Lu, X.; Wu, J.; Tong, W.; Lei, Q.; Fang, W., Interfacial Tensions for System of N-Heptane + Water with Quaternary Ammonium Surfactants and Additives of Nacl or C2–C4 Alcohols. *Journal of Chemical & Engineering Data* **2014,** *59* (3), 860-868.
(67) Comiskey, B.; Albert, J. D.; Yoshizawa, H.; Jacobson, J., An Electrophoretic Ink for All-Printed Reflective Electronic Displays. *Nature* **1998,** *394*, 253.
(68) General Overview of Food Hydrocolloids. In *Cellulose and Cellulose Derivatives in the Food Industry*, Wüstenberg, T., Ed. Wiley‐VCH Verlag GmbH & Co. KGaA: 2014; pp 1-68.
(69) Sworn, G., 8 - Xanthan Gum. In *Handbook of Hydrocolloids (Second Edition)*, Woodhead Publishing: 2009; pp 186-203.
(70) Huang, Y.-T.; Zhang, H.; Wan, X.-J.; Chen, D.-Z.; Chen, X.-F.; Ye, X.; Ouyang, X.; Qin, S.-Y.; Wen, H.-X.; Tang, J.-N., Carbon Nanotube-Enhanced Double-Walled Phase-Change Microcapsules for Thermal Energy Storage. *Journal of Materials Chemistry A* **2017,** *5* (16), 7482-7493.
(71) Reeves, R. E.; Barrett, B. J.; Mazzeno, L. W., The Heterogeneous Hydrolysis of Highly Methylated Cotton Cellulose. *Journal of the American Chemical Society* **1952,** *74* (18), 4491-4494.
(72) Vink, H., Degradation of Cellulose and Cellulose Derivatives by Acid Hydrolysis. *Die Makromolekulare Chemie* **1966,** *94* (1), 1-14.

(73) Rosell, K.-G., Location of Cellulose Substituents. In *Analysis of Carbohydrates by Glc and Ms*, 1st ed.; Biermann, C. J.; McGinnis, G. D., Eds. CRC Press: Florida, USA, 1988; pp 237-256.
(74) Armisén, R.; Gaiatas, F., 4 - Agar. In *Handbook of Hydrocolloids (Second Edition)*, Woodhead Publishing: 2009; pp 82-107.
(75) Voiges, K.; Lämmerhardt, N.; Distelrath, C.; Mischnick, P., Substituent Effects on the Kinetics of Acid-Catalyzed Hydrolysis of Methyl Cellulose. *Cellulose* **2017,** *24* (2), 555-569.
(76) Chang, K. Y., Interaction of Phenol with the Polysaccharide of Bacterial Cell Wall. *Biochemical and Biophysical Research Communications* **1973,** *51* (4), 900-906.
(77) Shiraishi, N., Wood Plasticization. In *Wood and Cellulosic Chemistry*, 2nd ed.; Hon, D. N.-S.; Shiraishi, N., Eds. Marcel Dekker, Inc.: Bosa Roca, United States, 2000; pp 655-700.
(78) Suvorova, O. B.; Iozep, A. A.; Passet, B. V., Reactions of Polysaccharide Aldehydes with Aromatic Hydroxy Compounds. *Russian Journal of Applied Chemistry* **2001,** *74* (11), 1933-1936.
(79) Rao, R. S. P.; Muralikrishna, G., Non-Starch Polysaccharide–Phenolic Acid Complexes from Native and Germinated Cereals and Millet. *Food Chemistry* **2004,** *84* (4), 527-531.
(80) Raeesi, M.; Mirabedini, S. M.; Farnood, R. R., Preparation of Microcapsules Containing Benzoyl Peroxide Initiator with Gelatin-Gum Arabic/Polyurea-Formaldehyde Shell and Evaluating Their Storage Stability. *ACS Applied Materials & Interfaces* **2017,** *9* (24), 20818-20825.
(81) Bull, H. B.; Breese, K., Water and Solute Binding by Proteins: 1. Electrolytes. *Archives of Biochemistry and Biophysics* **1970,** *137* (2), 299-305.
(82) Bull, H. B.; Breese, K., Water and Solute Binding by Proteins: Ii. Denaturants. *Archives of Biochemistry and Biophysics* **1970,** *139* (1), 93-96.
(83) Torrestiana, B.; Galindo, E.; Brito, E., Cooperative Binding of Sucrose in Xanthan Gum Solutions. *Biotechnology Progress* **1988,** *4* (1), 1-5.
(84) Bagger, H. L.; Fuglsang, C. C.; Westh, P., Preferential Binding of Two Compatible Solutes to the Glycan Moieties of Peniophora Lycii Phytase. *Biochemistry* **2003,** *42* (34), 10295-10300.
(85) Rondeau-Mouro, C.; Zykwinska, A.; Durand, S.; Doublier, J.-L.; Buléon, A., Nmr Investigations of the 4-Ethyl Guaicol Self-Diffusion in Iota (I)-Carrageenan Gels. *Carbohydrate Polymers* **2004,** *57* (4), 459-468.
(86) Elsabee, M. Z.; Morsi, R. E.; Al-Sabagh, A. M., Surface Active Properties of Chitosan and Its Derivatives. *Colloids and Surfaces B: Biointerfaces* **2009,** *74* (1), 1-16.
(87) Guo, H.; Zhao, X.; Wang, J., Synthesis of Functional Microcapsules Containing Suspensions Responsive to Electric Fields. *Journal of Colloid and Interface Science* **2005,** *284* (2), 646-651.
(88) Hofmeister, I.; Landfester, K.; Taden, A., Controlled Formation of Polymer Nanocapsules with High Diffusion-Barrier Properties and Prediction of Encapsulation Efficiency. *Angewandte Chemie International Edition* **2015,** *54* (1), 327-330.
(89) Zhang, Z., Mechanical Strength of Single Microcapsules Determined by a Novel Micromanipulation Technique. *Journal of Microencapsulation* **1999,** *16* (1), 117-124.
(90) Johnson, K. L., *Contact Mechanics*. Cambridge University Press: Cambridge, United Kingdom, 1985.
(91) Kuo-Kang, L., Deformation Behaviour of Soft Particles: A Review. *Journal of Physics D: Applied Physics* **2006,** *39* (11), R189.
(92) Maier, G., Gas Separation with Polymer Membranes. *Angewandte Chemie International Edition* **1998,** *37* (21), 2960-2974.

(93) Hawlader, M. N. A.; Uddin, M. S.; Khin, M. M., Microencapsulated Pcm Thermal-Energy Storage System. *Applied Energy* **2003,** *74* (1), 195-202.
(94) Zhang, Y.; Zheng, X.; Wang, H.; Du, Q., Encapsulated Phase Change Materials Stabilized by Modified Graphene Oxide. *Journal of Materials Chemistry A* **2014,** *2* (15), 5304-5314.
(95) *Perry's Chemical Engineers' Handbook.* 7th ed.; McGraw-Hill: 1997.
(96) Sebastian, K.; Jan, K., Secondary Polygonal Instability of Buckled Spherical Shells. *EPL (Europhysics Letters)* **2014,** *106* (2), 24004.
(97) Takemori, M. T., Polymer Fatigue. *Annual Review of Materials Science* **1984,** *14* (1), 171-204.
(98) Peng, W.; Riedl, B., Thermosetting Resins. *Journal of Chemical Education* **1995,** *72* (7), 587.
(99) Hertzberg, R. W.; Vinci, R. P.; Hertzberg, J. L., Elastic Response of Solids. In *Deformation and Fracture Mechanics of Engineering Materials*, 5th ed.; Jennifer, W., Ed. John Wiley & Sons, Inc: 2012; pp 3-61.

(53) Fang, G.; Li, H.; Yang, F.; Liu, X.; Wu, S., Preparation and Characterization of Nano-Encapsulated N-Tetradecane as Phase Change Material for Thermal Energy Storage. *Chemical Engineering Journal* **2009,** *153* (1), 217-221.
(54) Salaün, F.; Devaux, E.; Bourbigot, S.; Rumeau, P., Influence of Process Parameters on Microcapsules Loaded with N-Hexadecane Prepared by in Situ Polymerization. *Chemical Engineering Journal* **2009,** *155* (1), 457-465.
(55) Mao, J.; Yang, H.; Zhou, X., In Situ Polymerization of Uniform Poly(Urea–Formaldehyde) Microcapsules Containing Paraffins under the High-Speed Agitation without Emulsifier. *Polymer Bulletin* **2012,** *69* (6), 649-660.
(60) Tseng, Y. H.; Fang, M. H.; Tsai, P. S.; Yang, Y. M., Preparation of Microencapsulated Phase-Change Materials (Mcpcms) by Means of Interfacial Polycondensation. *Journal of Microencapsulation* **2005,** *22* (1), 37-46.
(61) Boh, B.; Knez, E.; Staresinic, M., Microencapsulation of Higher Hydrocarbon Phase Change Materials by in Situ Polymerization. *Journal of Microencapsulation* **2005,** *22* (7), 715-735.
(62) Chen, Z.; Cao, L.; Fang, G.; Shan, F., Synthesis and Characterization of Microencapsulated Paraffin Microcapsules as Shape-Stabilized Thermal Energy Storage Materials. *Nanoscale and Microscale Thermophysical Engineering* **2013,** *17* (2), 112-123.
(63) Zhang, H.; Wang, X., Fabrication and Performances of Microencapsulated Phase Change Materials Based on N-Octadecane Core and Resorcinol-Modified Melamine–Formaldehyde Shell. *Colloids and Surfaces A: Physicochemical and Engineering Aspects* **2009,** *332* (2), 129-138.
(107) Olea, A. F.; Thomas, J. K., Rate Constants for Reactions in Viscous Media: Correlation between the Viscosity of the Solvent and the Rate Constant of the Diffusion-Controlled Reactions. *Journal of the American Chemical Society* **1988,** *110* (14), 4494-4502.
(108) Friedman, M. H., Free Diffusion. In *Principles and Models of Biological Transport*, 2 ed.; Springer-Verlab: New York, 2008; pp 29-65.